Hindawi Publishing Corporation
Advances in High Energy Physics
Volume 2013, Article ID 371908, 20 pages
http://dx.doi.org/10.1155/2013/371908

Review Article

Some Aspects of Anisotropic Quark-Gluon Plasma

Mahatsab Mandal and Pradip Roy

Saha Institute of Nuclear Physics, 1/AF Bidhannagar, Kolkata 700064, India

Correspondence should be addressed to Mahatsab Mandal; mahatsab.mandal@saha.ac.in

Received 5 April 2013; Revised 5 July 2013; Accepted 19 July 2013

Academic Editor: Edward Sarkisyan-Grinbaum

We review the various aspects of anisotropic quark-gluon plasma (AQGP) that have recently been discussed by a number of authors. In particular, we focus on the electromagnetic probes of AQGP, inter quark potential, quarkonium states in AQGP, and the nuclear modifications factor of various bottomonium states using this potential. In this context, we will also discuss the radiative energy loss of partons and nuclear modification factor of light hadrons in the context of AQGP. The features of the wake potential and charge density due to the passage of jet in AQGP will also be demonstrated.

1. Introduction

Ever since the possibility of creating the quark-gluon plasma (QGP) in relativistic heavy ion collision was envisaged, numerous indirect signals were proposed to probe the properties of such an exotic state of matter. For example, electromagnetic probes (photon and dilepton) [1], J/ψ suppression [2], jet quenching vis-a-vis energy loss [3–10], and many more. In spite of these, many properties of the QGP are poorly understood. The most pertinent question is whether the matter produced in relativistic heavy ion collisions is in thermal equilibrium or not. Studies on elliptical flow (up to about $p_T \sim 1.5$ GeV) using ideal hydrodynamics indicate that the matter produced in such collisions becomes isotropic with $\tau_{\text{iso}} \sim 0.6$ fm/c [11–13]. On the other hand, using second-order transport coefficients with conformal field theory, it has been found that the isotropization/thermalization time has sizable uncertainties [14] leading to uncertainties in the initial conditions, such as the initial temperature.

In the absence of a theoretical proof favoring the rapid thermalization and the uncertainties in the hydrodynamical fits of experimental data, it is very hard to assume hydrodynamical behavior of the system from the very beginning. The rapid expansion of the matter along the beam direction causes faster cooling in the longitudinal direction than in the transverse direction [18]. As a result, the system becomes anisotropic with $\langle {p_L}^2 \rangle \ll \langle {p_T}^2 \rangle$ in the local rest frame. At some later time when the effect of parton interaction rate overcomes the plasma expansion rate, the system returns to the isotropic state again and remains isotropic for the rest of the period. If the QGP, just after formation, becomes anisotropic, soft unstable modes are generated characterized by the exponential growth of the transverse chromomagnetic/chromoelectric fields at short times. Thus, it is very important to study the collective modes in an AQGP and use these results to calculate relevant observables. The instability, thus developed, is analogous to QED Weibel instability. The most important collective modes are those which correspond to transverse chromomagnetic field fluctuations, and these have been studied in great detail in [19–26]. This is known as chromo-Weibel instability, and it differs from its QED analogue because of nonlinear gauge self-interactions. Because of this fact, anisotropy driven plasma instabilities in QCD may slow down the process of isotropization whereas, in QED, it can speed up the process [27].

To characterize the presence of initial state of momentum space anisotropy, it has been suggested to look for some observables which are sensitive to the early time after the collision. The effects of preequilibrium momentum anisotropy on various observables have been studied quite extensively over the past few years. The collective oscillations in an AQGP have been studied in [28, 29]. Heavy quark energy loss and momentum broadening in anisotropic QGP have been investigated in [30, 31]. However, the radiative energy loss of partons in AQGP has recently been calculated in [32]. Another aspect of jet propagation in hot and dense medium

is the wake that it creates along its path. First, Ruppert and Muller [33] have investigated that when a jet propagates through the medium, a wake of current and charge density is induced which can be studied within the framework of linear-response theory. The result shows the wake in both the induced charge and current density due to the screening effect of the moving parton. In the quantum liquid scenario, the wake exhibits an oscillatory behavior when the charge parton moves very fast. Later, Chakraborty et al. [34] also found the oscillatory behavior of the induced charge wake in the backward direction at a large parton speed using HTL perturbation theory. In a collisional quark-gluon plasma, it is observed that the wake properties change significantly compared to the collisionless case [35]. Recently, Jiang and Li [36, 37] have investigated the color response wake in the viscous QGP with the HTL resummation technique. It is shown that the increase of the shear viscosity enhances the oscillation of the induced charge density as well as the wake potential. The effect of momentum space anisotropy on the wake potential and charge density has recently been considered in [38].

Effects of anisotropy on photon and dilepton yields have been investigated rigorously in [16, 39–43]. Recently, the authors in [44] calculated the nuclear modification factor for light hadrons assuming an anisotropic QGP and showed how the isotropization time can be extracted by comparing with the experimental data.

The organization of the review is as follows. In Section 2 we will briefly discuss various models of space-time evolution in AQGP along with the electromagnetic probes which can be used to extract the isotropization time of the plasma. Section 3 will be devoted to discuss the works on heavy quark potential and related phenomena (such as gluon J/ψ dissociation cross-section in an AQGP) that have been investigated so far. We will also discuss the radiative energy loss of partons in AQGP and nuclear modification factor of light hadrons due to the energy loss of the jet in Section 4. In Section 5, the effect of momentum anisotropy on wake potential and charge density due to the passage of a jet will be presented. Finally we summarize in Section 6.

2. Electromagnetic Probes

Photons and dileptons have long been considered to be the good probes to characterize the initial stages of heavy ion collisions as these interact "weakly" with the constituents of the medium and can come out without much distortion in their energy and momentum. Thus, they carry the information about the space-time point where they are produced. Since anisotropy is an early stage phenomena, photons and dileptons are the efficient probes to characterize this stage. The yield of dileptons (henceforth called medium dileptons/photons) in an AQGP has been calculated using a phenomenological model of space-time evolution in (1 + 1) dimension [42, 43]. This model (henceforth referred to as model I) introduces two parameters: p_{hard} and ξ which are functions of time. The former is called the hard momentum scale and is related to the average momentum of the particles in the medium. In isotropic case this can be identified with the temperature of the system. The latter is called the anisotropy parameter and $-1 < \xi < \infty$. Furthermore, the model interpolates between early-time 1 + 1 free streaming behavior ($\tau \ll \tau_{\text{iso}}$) and late-time ideal hydrodynamical behavior ($\tau \gg \tau_{\text{iso}}$). We first discuss various space-time evolution models of AQGP. In model I the time dependence of ξ is given by [42, 43]

$$\xi(\tau, \delta) = \left(\frac{\tau}{\tau_i}\right)^{\delta} - 1, \tag{1}$$

where the exponent $\delta = 2(2/3)$ corresponds to free streaming (collisionally broadened) preequilibrium state momentum space anisotropy and $\delta = 0$ corresponds to thermalization. τ_i is the formation time of the QGP. For smooth transition from free streaming to hydrodynamical behavior a transition width γ^{-1} is introduced. The time dependences of various relevant parameters are obtained in terms of a smeared step function [42, 43] as follows:

$$\lambda(\tau) = \frac{1}{2}\left(\tanh\left[\frac{\gamma(\tau - \tau_{\text{iso}})}{\tau_i}\right] + 1\right). \tag{2}$$

For $\tau \ll \tau_{\text{iso}}$ ($\gg \tau_{\text{iso}}$), we have $\lambda = 0(1)$ which corresponds to free streaming (hydrodynamics). Thus, the time dependences of ξ and p_{hard} are as follows [42, 43]:

$$\begin{aligned} \xi(\tau, \delta) &= \left(\frac{\tau}{\tau_i}\right)^{\delta(1-\lambda(\tau))} - 1, \\ p_{\text{hard}}(\tau) &= T_i \overline{\mathcal{U}}^{1/3}(\tau), \end{aligned} \tag{3}$$

where

$$\begin{aligned} \mathcal{U}(\tau) &\equiv \left[\mathcal{R}\left(\left(\frac{\tau_{\text{iso}}}{\tau}\right)^{\delta} - 1\right)\right]^{3\lambda(\tau)/4} \left(\frac{\tau_{\text{iso}}}{\tau}\right)^{1-\delta(1-\lambda(\tau))/2}, \\ \overline{\mathcal{U}} &\equiv \frac{\mathcal{U}(\tau)}{\overline{\mathcal{U}}(\tau_i)}, \\ \mathcal{R}(x) &= \frac{1}{2}\left[\frac{1}{(x+1)} + \frac{\tan^{-1}\sqrt{x}}{\sqrt{x}}\right], \end{aligned} \tag{4}$$

and T_i is the initial temperature of the plasma. In our calculation, we assume a fast-order phase transition beginning at the time τ_f and ending at $\tau_H = r_d \tau_f$, where $r_d = g_Q/g_H$ is the ratio of the degrees of freedom in the two (QGP phase and hadronic phase) phases and τ_f is obtained by the condition $p_{\text{hard}}(\tau_f) = T_c$, which we take as 192 MeV. We also include the contribution from the mixed phase.

The other model (referred to as model II hereafter) of space-time evolution of highly AQGP is the boost invariant dissipative dynamics in (0 + 1) dimension [45]. This model can reproduce both the hydrodynamics and the free streaming limits. The time evolution of the phase space distribution $f(t, z, \mathbf{p})$ can be described by Boltzmann equation. Thus, as a starting point, we write the Boltzmann equation in (0 + 1) dimension in the lab frame as follows:

$$p^t \partial_t f(t, z, \mathbf{p}) + p^z \partial_z f(t, z, \mathbf{p}) = -\mathcal{C}\left[f(t, z, \mathbf{p})\right], \tag{5}$$

where homogeneity in the transverse direction is assumed and $\mathscr{C}[f(t,z,\mathbf{p})]$ is the collision kernel. We assume that the phase-space distribution for the anisotropic plasma is given by the following ansatz [28, 29]:

$$f\left(\mathbf{p},\xi\left(\tau\right),p_{\text{hard}}\left(\tau\right)\right)=f_{\text{iso}}\left(\frac{\left[\mathbf{p}^2+\xi\left(\tau\right)\left(\mathbf{p}\cdot\widehat{\mathbf{n}}\right)\right]^2}{p_{\text{hard}}^2\left(\tau\right)}\right), \quad (6)$$

where $\widehat{\mathbf{n}}$ is the direction of anisotropy. Note that, in subsequent sections, this distribution function will be used to calculate various observables. Now it is convenient to write (5) in the comoving frame. Introducing space-time rapidity (Θ), particle rapidity (y), and proper time (τ) one can write (5) in terms of the comoving coordinates as [45]

$$\begin{aligned}&\left(p_T\cosh\left(y-\Theta\right)\frac{\partial}{\partial\tau}+\frac{p_T\sinh\left(y-\Theta\right)}{\tau}\frac{\partial}{\partial\tau}\right)\\&\quad\times f\left(\mathbf{p},\xi,p_{\text{hard}}\right)\\&=-\Gamma p_T\cosh\left(y-\Theta\right)\left[f\left(\mathbf{p},\xi,p_{\text{hard}}\right)-f_{\text{eq}}\left(\mathbf{p},T\left(\tau\right)\right)\right],\end{aligned} \quad (7)$$

where $\Gamma=2T(\tau)/(5\overline{\eta})$ and $\overline{\eta}=\eta/s$, η is the shear viscosity coefficient.

The zeroth-order and first-order moments of the Boltzmann equation give the time dependence for ξ and p_{hard} as described in [45]. Without going into further details we simply quote the coupled differential equations that have to be solved to get the time dependence of ξ and p_{hard} [45] as follows:

$$\begin{aligned}&\frac{1}{1+\xi}\partial_\tau\xi=\frac{2}{\tau}-4\Gamma\mathscr{R}\left(\xi\right)\frac{\mathscr{R}^{3/4}\sqrt{1+\xi}-1}{2\mathscr{R}\left(\xi\right)+3\left(1+\xi\right)\mathscr{R}'\left(\xi\right)},\\&\frac{1}{1+\xi}\frac{1}{p_{\text{hard}}}\partial_\tau p_{\text{hard}}\\&\quad=\frac{2}{\tau}-4\Gamma\mathscr{R}'\left(\xi\right)\frac{\mathscr{R}^{3/4}\sqrt{1+\xi}-1}{2\mathscr{R}\left(\xi\right)+3\left(1+\xi\right)\mathscr{R}'\left(\xi\right)}.\end{aligned} \quad (8)$$

The previous two coupled differential equations have to be solved numerically. The results are shown in Figure 1. It is seen that the anisotropy parameter falls much rapidly compared to the case when model II is used. There is a narrow window in τ where ξ dominates in case of model I. The cooling is slower in case of model II as can be seen from the right panel of Figure 1. These observations have important consequence on various observables.

The assumption of boost invariant in the longitudinal direction can be relaxed and such a space-time model (the so called AHYDRO) has been proposed in [46]. As before, the time evolutions of various quantities can be obtained by taking moments of the Boltzmann equation. However, in this case, instead of two one obtains three coupled differential equations. The third variable is the longitudinal flow velocity (see [46] for details). The observations of this work are as follows. It removes the problem of negative longitudinal pressure sometimes obtained in 2nd-order viscous hydrodynamics and this model leads to much slower relaxation towards isotropy. In this review, for the sake of simplicity, the observables of AQGP will be calculated using space-time model I. The same can also be calculated using other space-time models of AQGP, and the results may differ from case to case.

2.1. Photons. We first consider the medium photon production from AQGP. The detail derivation of the differential rate is standard and can be found in [16, 39–41]. Here we will quote only the final formula for total photon yield after convoluting with the space-time evolution. The total medium photon yield, arising from the pure QGP phase and the mixed phase is given by

$$\begin{aligned}\frac{dN^\gamma}{dyd^2p_T}=\pi R_\perp^2\left[\int_{\tau_{\text{i}}}^{\tau_f}\tau\,d\tau\int d\eta\frac{dN^\gamma}{d^4xdyd^2p_T}\right.\\\left.+\int_{\tau_f}^{\tau_H}f_{\text{QGP}}\left(\tau\right)\tau\,d\tau\int d\eta\frac{dN^\gamma}{d^4xdyd^2p_T}\right],\end{aligned} \quad (9)$$

where $f_{\text{QGP}}(\tau)=(r_d-1)^{-1}(r_d\tau_f\tau^{-1}-1)$ is the fraction of the QGP phase in the mixed phase [47] and $R_\perp=1.2A^{1/3}$ fm is the radius of the colliding nucleus in the transverse plane. The energy of the photon in the fluid rest frame is given by $E_\gamma=p_T\cosh(y-\Theta)$, where Θ and y are the space-time and photon rapidities, respectively. The anisotropy parameter and the hard momentum scale enter through the differential rate via $dN^\gamma/d^4xdyd^2p_T$ (see [16, 39–41] for details).

We plot the total photon yield coming from thermal QGP, thermal hadrons and the initial hard contribution in Figure 2 and compare it with the RHIC data for various values of τ_{iso}. In the hadronic sector, we include photons from baryon-meson (BM) and meson-meson (MM) reactions. Two scenarios have been considered: (i) pure hydrodynamics from the beginning and (ii) inclusion of momentum state anisotropy. We observe that (i) photons from BM reactions are important, (ii) pure hydro is unable to reproduce the data, that is, some amount of momentum anisotropy is needed, and (iii) exclusion of BM reactions underpredict the data. We note that the value of τ_{iso} needed to describe the data also lies in the range $1.5\,\text{fm/c}\geq\tau_{\text{iso}}\geq 0.5\,\text{fm/c}$ for both values of the transition temperatures.

2.2. Dileptons. The dilepton production from AQGP has been estimated in [17, 42, 43] using the same space-time model. It is argued in [17] that the transverse momentum distribution of lepton pair in AQGP could provide a good insight about the estimation of τ_{iso}. We will briefly discuss the high mass dilepton yield along with the p_T distribution in AQGP. Here we consider only the QGP phase as in the high mass region the yield from the hadronic reactions and decay should be suppressed. The dilepton production from quark-antiquark annihilation can be calculated from kinetic theory and is given by

$$\begin{aligned}&E\frac{dR}{d^3P}\\&\quad=\int\frac{d^3\mathbf{p}_1}{\left(2\pi\right)^3}\frac{d^3\mathbf{p}_2}{\left(2\pi\right)^3}f_q\left(\mathbf{p}_1\right)f_{\overline{q}}\left(\mathbf{p}_2\right)v_{q\overline{q}}\sigma_{q\overline{q}}^{l^+l^-}\delta^{(4)}\left(P-p_1-p_2\right),\end{aligned} \quad (10)$$

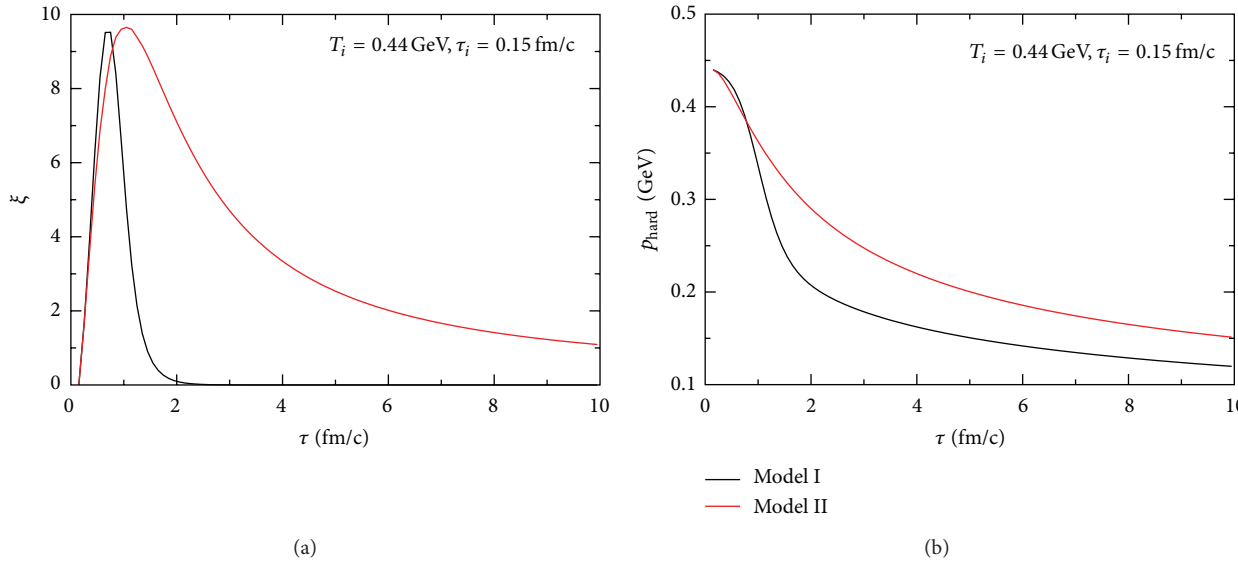

FIGURE 1: (Color online) Time evolutions of (a) the anisotropy parameter ξ and (b) the hard momentum scale p_{hard} in the two space-time models described in the text. The graphs are taken from [15].

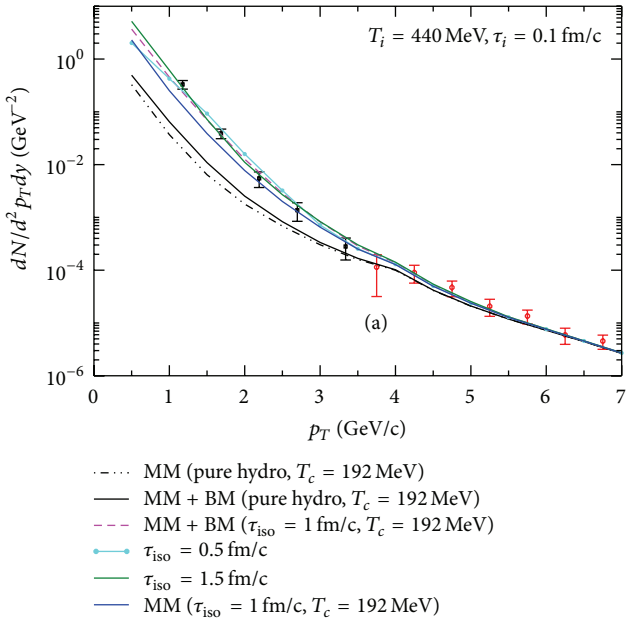

FIGURE 2: (Color online) Photon transverse momentum distributions at RHIC energies. The initial conditions are taken as T_i = 440 MeV, τ_i = 0.1 fm/c, and T_c = 192 MeV [16].

where $f_{q(\bar{q})}$ is the phase space distribution function of the medium quarks (anti-quarks), $v_{q\bar{q}}$ is the relative velocity between quark and anti-quark, and $\sigma_{q\bar{q}}^{l^+l^-}$ is the total cross-section. Consider

$$\sigma_{q\bar{q}}^{l^+l^-} = \frac{4\pi}{3}\frac{\alpha^2}{M^2}\left(1+\frac{2m_l^2}{M^2}\right)\left(1-\frac{4m_l^2}{M^2}\right)^{1/2}. \tag{11}$$

Using the anisotropic distribution functions for the quark (antiquark) defined earlier the differential dilepton production rate can be written as [43]

$$\begin{aligned}\frac{dR}{d^4P} &= \frac{5\alpha^2}{18\pi^5}\times\int_{-1}^{1} d\left(\cos\theta_{p_1}\right)\\ &\times\int_{a_+}^{a_-}\frac{dp_1}{\sqrt{\chi}}\; p_1 f_q\left(\sqrt{\mathbf{p}_1^2\left(\mathbf{1}+\xi\cos^2\theta_{\mathbf{p}_1}\right)}, p_{\text{hard}}\right)\\ &\times f_{\bar{q}}\left(\sqrt{\left(\mathbf{E}-\mathbf{p}_1\right)^2+\xi\left(\mathbf{p}_1\cos\theta_{\mathbf{p}_1}-\mathbf{P}\cos\theta_{\mathbf{P}}\right)^2}, p_{\text{hard}}\right).\end{aligned} \tag{12}$$

The invariant mass and p_T distributions of lepton pair can be obtained after space-time integration using the evolution model described earlier. The final rates are as follows [17]:

$$\begin{aligned}\frac{dN}{dM^2dy} &= \pi R_\perp^2\int d^2P_T\int_{\tau_i}^{\tau_f}\int_{-\infty}^{\infty}\frac{dR}{d^4P}\tau d\tau\, d\eta,\\ \frac{dN}{d^2P_T dy} &= \pi R_\perp^2\int dM^2\int_{\tau_i}^{\tau_f}\int_{-\infty}^{\infty}\frac{dR_{\text{ann}}}{d^4P}\tau d\tau\, d\eta.\end{aligned} \tag{13}$$

The numerical results are shown in Figure 3 for the initial conditions τ_i = 0.88 fm/c and T_i = 845 MeV corresponding to the LHC energies. For $\tau_{\text{iso}} \sim$ 2 fm/c, it is observed that the dilepton yield from AQGP is comparable to Drell-Yan process. The p_T distribution shows (Figure 3(b)) that the medium contribution dominates over all the other contributions upto $p_T \sim$ 9 GeV. The extraction of the isotropization time can only be determined if these results are confronted with the data after the contributions from

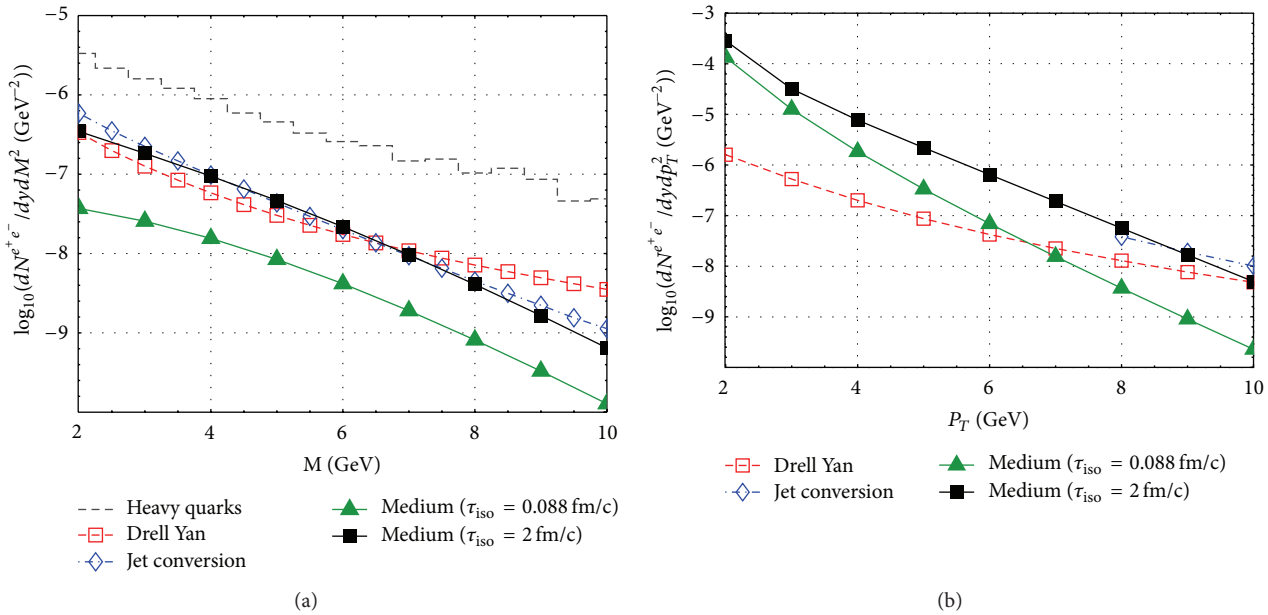

FIGURE 3: (Color online) Invariant mass (a) and momentum (b) distribution of midrapidity dileptons in central Pb + Pb collisions at LHC. The figures are taken from [17].

the semileptonic decay from heavy quarks and Drell-Yan processes are subtracted from the total yield.

3. Heavy Quark Potential and Quarkonium States in AQGP

In this section, we will discuss the heavy quark potential in AQGP that has been calculated in [48]. It is to be noted that this formalism will enable us to calculate the radiative energy loss of both heavy and light quarks, and this will be discussed in Section 4. To calculate the interquark potential one starts with the retarded gluon self-energy expressed as [49]

$$\Pi^{\mu\nu}(K) = g^2 \int \frac{d^3p}{(2\pi)^3} P^{\mu} \frac{\partial f(\mathbf{p})}{\partial P_{\beta}} \left(g^{\beta\nu} - \frac{P^{\nu} K^{\beta}}{K \cdot P + i\varepsilon} \right). \quad (14)$$

This tensor is symmetric, $\Pi^{\mu\nu}(K) = \Pi^{\nu\mu}(K)$, and transverse, $K_{\mu}\Pi^{\mu\nu}(K) = 0$. The spatial components of the self-energy tensor can be written as

$$\Pi^{ij}(K) = -g^2 \int \frac{d^3p}{(2\pi)^3} v^i \partial^l f(\mathbf{p}) \left(\delta^{jl} + \frac{v^j k^l}{K \cdot V + i\varepsilon} \right), \quad (15)$$

where $f(\mathbf{p})$ is the arbitrary distribution function. To include the local anisotropy in the plasma, one has to calculate the gluon polarization tensor incorporating anisotropic distribution function of the constituents of the medium. We assume that the phase-space distribution for the anisotropic plasma is given by (6). Using the ansatz for the phase space distribution given in (6), one can simplify (15) to

$$\Pi^{ij}(K) = m_D^2 \int \frac{d\Omega}{(4\pi)} v^i \frac{v^l + \xi(\mathbf{v} \cdot \hat{\mathbf{n}}) n^l}{\left(1 + \xi(\mathbf{v} \cdot \hat{\mathbf{n}})^2\right)^2} \left(\delta^{jl} + \frac{v^j k^l}{K \cdot V + i\varepsilon} \right), \quad (16)$$

where m_D is the Debye mass for isotropic medium represented by

$$m_D^2 = -\frac{g^2}{2\pi^2} \int_0^{\infty} dp p^2 \frac{df_{\text{iso}}(p^2)}{dp}. \quad (17)$$

Due to the anisotropy direction, the self-energy, apart from momentum $\mathbf{k}$, also depends on the anisotropy vector $\mathbf{n}$, with $n^2 = 1$. Using the proper tensor basis [28], one can decompose the self-energy into four structure functions as

$$\Pi^{ij}(k) = \alpha A^{ij} + \beta B^{ij} + \gamma C^{ij} + \delta D^{ij}, \quad (18)$$

where

$$A^{ij} = \delta^{ij} - \frac{k^i k^j}{k^2}, \qquad B^{ij} = k^i k^j,$$
$$C^{ij} = \frac{\tilde{n}^i \tilde{n}^j}{\tilde{n}^2}, \qquad D^{ij} = k^i \tilde{n}^j + \tilde{n}^i k^j, \quad (19)$$

with $\tilde{n}^i = A^{ij} n^j$ which obeys $\tilde{n} \cdot k = 0$. α, β, γ, and δ are determined by the following contractions:

$$k^i \Pi^{ij} k^j = \mathbf{k}^2 \beta, \qquad \tilde{n}^i \Pi^{ij} k^j = \tilde{n}^2 \mathbf{k}^2 \delta,$$
$$\tilde{n}^i \Pi^{ij} \tilde{n}^j = \tilde{n}^2 (\alpha + \gamma), \qquad \text{Tr}\, \Pi^{ij} = 2\alpha + \beta + \gamma. \quad (20)$$

Before going to the calculation of the quark-quark potential let us study the collective modes in AQGP which have been thoroughly investigated in [28, 29], and we briefly discuss this here. The dispersion law for the collective modes of anisotropic plasma in temporal axial gauge can be determined by finding the poles of propagator Δ^{ij} as follows:

$$\Delta^{ij}(K) = \frac{1}{\left[(\mathbf{k}^2 - \omega^2) \delta^{ij} - k^i k^j + \Pi^{ij}(k) \right]}. \quad (21)$$

Substituting (19) in the previous equation and performing the inverse formula [28], one finds

$$\Delta(K) = \Delta_A[\mathbf{A} - \mathbf{C}] + \Delta_G\left[\left(\mathbf{k}^2 - \omega^2 + \alpha + \gamma\right)\mathbf{B} + \left(\beta - \omega^2\right)\mathbf{C} - \delta\mathbf{D}\right]. \tag{22}$$

The dispersion relation for the gluonic modes in anisotropic plasma is given by the zeros of

$$\Delta_A^{-1}(k) = k^2 - \omega^2 + \alpha = 0,$$
$$\Delta_G^{-1}(k) = \left(k^2 - \omega^2 + \alpha + \gamma\right)\left(\beta - \omega^2\right) - k^2\widehat{n}^2\delta^2 = 0. \tag{23}$$

Let us first consider the stable modes for real $\omega > k$ in which case there are at most two stable modes stemming from $\Delta_G^{-1} = 0$. The other stable mode comes from zero of Δ_A^{-1}. Thus, for finite ξ, there are three stable modes. Note that these modes depend on the angle of propagation with respect to the anisotropy axis. The dispersion relation for the unstable modes can be obtained by letting $\omega \to i\Gamma$ in $\Delta_G^{-1} = 0$ and Δ_A^{-1} leading to two unstable modes and these modes again depend the direction of propagation with respect to the anisotropy axis.

The collective modes in a collisional AQGP have been investigated in [50] using Bhatnagar-Gross-Krook collisional kernel. It has been observed that inclusion of the collisions slows down the growth rate of unstable modes and the instabilities disappear at certain critical values of the collision frequency.

In order to calculate the quark-quark potential, we resort to the covariant gauge. Using the previous expression for gluon self-energy in anisotropic medium the propagator, in covariant gauge, can be calculated after some cumbersome algebra [48] as follows:

$$\Delta^{\mu\nu} = \frac{1}{(K^2 - \alpha)}\left[A^{\mu\nu} - C^{\mu\nu}\right] + \Delta_G\left[\left(K^2 - \alpha - \gamma\right)\frac{\omega^4}{K^4}B^{\mu\nu} + \left(\omega^2 - \beta\right)C^{\mu\nu} + \delta\frac{\omega^2}{K^2}D^{\mu\nu}\right] - \frac{\lambda}{K^4}K^\mu K^\nu, \tag{24}$$

where

$$\Delta_G^{-1} = \left(K^2 - \alpha - \gamma\right)\left(\omega^2 - \beta\right) - \delta^2\left[K^2 - (n\cdot K)^2\right]. \tag{25}$$

The structure functions (α, β, γ, and δ) depend on ω, $\mathbf{k}$, ξ, and on the angle (θ_n) between the anisotropy vector and the momentum $\mathbf{k}$. In the limit $\xi \to 0$, the structure functions γ and δ are identically zero, and α and β are directly related to the isotropic transverse and longitudinal self-energies, respectively [28]. In anisotropic plasma, the two-body interaction, as expected, becomes direction dependent. Now the momentum space potential can be obtained from the static gluon propagator in the following way [32, 48]:

$$V(k_\perp, k_z, \xi) = g^2\Delta^{00}(\omega = 0, k_\perp, k_z, \xi) = g^2\frac{\mathbf{k}^2 + m_\alpha^2 + m_\gamma^2}{\left(\mathbf{k}^2 + m_\alpha^2 + m_\gamma^2\right)\left(\mathbf{k}^2 + m_\beta^2\right) - m_\delta^2}, \tag{26}$$

where

$$m_\alpha^2 = -\frac{m_D^2}{2k_\perp^2\sqrt{\xi}} \times\left[k_z^2\tan^{-1}\left(\sqrt{\xi}\right) - \frac{k_z\mathbf{k}^2}{\sqrt{\mathbf{k}^2 + \xi k_\perp^2}} \times\tan^{-1}\left(\frac{\sqrt{\xi}k_z}{\sqrt{\mathbf{k}^2 + \xi k_\perp^2}}\right)\right],$$

$$m_\beta^2 = m_D^2\left(\left(\sqrt{\xi} + (1+\xi)\tan^{-1}\left(\sqrt{\xi}\right)\left(\mathbf{k}^2 + \xi k_\perp^2\right) + \xi k_z\left(\xi k_z + \left(\mathbf{k}^2(1+\xi)/\sqrt{\mathbf{k}^2 + \xi k_\perp^2}\right) \times\tan^{-1}\left(\sqrt{\xi}k_z/\sqrt{\mathbf{k}^2 + \xi k_\perp^2}\right)\right)\right) \times\left(2\sqrt{\xi}(1+\xi)\left(\mathbf{k}^2 + \xi k_\perp^2\right)\right)^{-1}\right), \tag{27}$$

$$m_\gamma^2 = -\frac{m_D^2}{2}\left(\frac{\mathbf{k}^2}{\mathbf{k}^2 + \xi k_\perp^2} - \frac{1 + 2k_z^2/k_\perp^2}{\sqrt{\xi}}\tan^{-1}\left(\sqrt{\xi}\right) + \frac{k_z\mathbf{k}^2\left(2\mathbf{k}^2 + 3\xi k_\perp^2\right)}{\sqrt{\xi}\left(\mathbf{k}^2 + \xi k_\perp^2\right)^{3/2}k_\perp^2} \times\tan^{-1}\left(\frac{\sqrt{\xi}k_z}{\sqrt{\mathbf{k}^2 + \xi k_\perp^2}}\right)\right),$$

$$m_\delta^2 = -\frac{\pi m_D^2\xi k_z k_\perp|\mathbf{k}|}{4\left(\mathbf{k}^2 + \xi k_\perp^2\right)^{3/2}},$$

where $\alpha_s = g^2/4\pi$ is the strong coupling constant, and we assume constant coupling. The coordinate space potential can be obtained by taking Fourier transform of (26):

$$V(\mathbf{r}, \xi) = -g^2C_F\int\frac{d^3k}{(2\pi)^3}e^{-i\mathbf{k}\cdot\mathbf{r}}V(k_\perp, k_z, \xi), \tag{28}$$

which, under small ξ limit, reduces to [48]

$$V(\mathbf{r}, \xi) \approx V_{\text{iso}}(r) - g^2C_F\xi m_D^2\int\frac{d^3k}{(2\pi)^3}e^{-i\mathbf{k}\cdot\mathbf{r}}\frac{2/3 - (\mathbf{k}\cdot\mathbf{n})^2/\mathbf{k}^2}{\left(\mathbf{k}^2 + m_D^2\right)^2}, \tag{29}$$

where $V_{\text{iso}}(r) = -g^2\ C_Fe^{-m_Dr}/(4\pi r)$. As indicated earlier, the potential depends on the angle between $\mathbf{r}$ and $\mathbf{n}$. When $\mathbf{r} \parallel \mathbf{n}$ the potential ($V_\parallel$) is given by [48]

$$V_\parallel(\mathbf{r}, \xi) = V_{\text{iso}}(r)\left[1 + \xi\left(2\frac{e^{\widehat{r}} - 1}{\widehat{r}^2} - \frac{2}{\widehat{r}} - 1 - \frac{\widehat{r}}{6}\right)\right], \tag{30}$$

whereas [48]

$$V_\perp(\mathbf{r}, \xi) = V_{\text{iso}}(r)\left[1 + \xi\left(\frac{1 - e^{\widehat{r}}}{\widehat{r}^2} + \frac{1}{\widehat{r}} + \frac{1}{2} + \frac{\widehat{r}}{3}\right)\right], \tag{31}$$

where $\widehat{r} = rm_D$.

For arbitrary ξ, (28) has to be evaluated numerically. It has been observed that because of the lower density of the plasma particles in AQGP, the potential is deeper and closer to the vacuum potential than for $\xi = 0$ [48]. This means that the general screening is reduced in an AQGP.

Next, we consider quarkonium states in an AQGP where the potential, to linear order in ξ, is given by (29) which can also be written as [51]

$$V(\mathbf{r},\xi) = V_{\text{iso}}(r)\left[1 - \xi\left(f_0(\hat{r}) + f_1(\hat{r})\cos 2\theta\right)\right], \tag{32}$$

where $\cos\theta = \hat{r}\cdot\hat{n}$ and the functions are given by [51]

$$f_0(\hat{r}) = \frac{6\left(1-e^{\hat{r}}\right)+\hat{r}\left[6-\hat{r}(\hat{r}-3)\right]}{12\hat{r}^2} = -\frac{\hat{r}}{6} - \frac{\hat{r}^2}{48} + \cdots,$$
$$f_1(\hat{r}) = \frac{6\left(1-e^{\hat{r}}\right)+\hat{r}\left[6+\hat{r}(\hat{r}+3)\right]}{12\hat{r}^2} = -\frac{\hat{r}^2}{16} + \cdots. \tag{33}$$

With the previous expressions, the real part of the heavy quark potential in AQGP, after finite quark mass correction, becomes [51]

$$V(\mathbf{r}) = -\frac{\alpha}{r}(1+\mu r)\exp(-\mu r) + \frac{2\sigma}{\mu}\left[1-\exp(-\mu r)\right] - \sigma r\exp(-\mu r) - \frac{0.8}{m_Q^2 r}, \tag{34}$$

where $\mu/m_D = 1 + \xi(3+\cos 2\theta)/16$ and the previous expression is the minimal extension of the KMS potential [52] in AQGP. The ground states and the excited states of the quarkonium states in AQGP have been found by solving the three-dimensional Schrodinger equation using the finite difference time domain method [53]. Without going into further details, we will quote the main findings of the work of [51]. The binding energies of charmonium and bottomonium states are obtained as a function of the hard momentum scale. For a fixed hard momentum scale, it is seen that the binding energy increases with anisotropy. Note that the potential (34) is obtained by replacing m_D by μ in KMS equation [52]. For a given hard momentum scale $\mu < m_D$, the quarkonium states are more strongly bound than the isotropic case. This implies that the dissociation temperature for a particular quarkonium state is more in AQGP. It is found that the dissociation temperature for J/ψ in AQGP is $1.4T_c$, whereas for isotropic case it is $1.2T_c$ [51].

Quarkonium binding energies have also been calculated using a realistic potential including the complex part in [54] by solving the 3D Schrodinger equation where the potential has the form

$$V(\mathbf{r},\xi) = V_R(\mathbf{r},\xi) + iV_I(\mathbf{r},\xi), \tag{35}$$

where the real part is given by (34) and the imaginary part is given in [55]. The main results of this calculations are as follows. For J/ψ, the dissociation temperature obtained in this case is $2.3T_c$ in isotropic case. It has been found that with anisotropy the dissociation temperature increases as the binding of quarkonium states becomes stronger in AQGP.

Thermal bottomonium suppression (R_{AA}) at RHIC and LHC energies has been calculated in [56, 57] in an AQGP. Two types of potentials have been considered there coming from the free energy (case A) and the internal energy (case B), respectively. By solving the 3D Schrodinger equation with these potentials, it has been found that the dissociation temperature for $\Upsilon(1s)$ becomes 373 MeV and 735 MeV for the cases A and B, respectively, whereas in case of $\xi = 0$, these becomes 298 MeV and 593 MeV. Thus, the dissociation temperature increases in case of AQGP irrespective of the choice of the potential. In case of other bottomonium states, the dissociation temperatures increase compared to the isotropic case. The nuclear modification factor has been calculated by coupling AHYDRO [46] with the solutions of Schrodinger equation. Introduction of AHYDRO into the picture makes p_{hard} and ξ functions of proper time (τ), transverse coordinate ($\mathbf{x}_\perp$), and the space-time rapidity (Θ). As a consequence, both the real and imaginary part of the binding energies become functions of τ, $\mathbf{x}_\perp$, and Θ. Now the nuclear modification factor (R_{AA}) is related to the decay rate (Γ) of the state in question, where $\Gamma = -2\mathcal{F}[E]$. Thus, R_{AA} is given by [56, 57]

$$R_{AA}(p_T,\mathbf{x}_\perp,\Theta) = e^{-\zeta(p_T,\mathbf{x}_\perp,\Theta)}, \tag{36}$$

where $\zeta(p_T,\mathbf{x}_\perp,\Theta)$ is given by

$$\zeta(p_T,\mathbf{x}_\perp,\Theta) = \theta\left(\tau_f - \tau_{\text{form}}\right)\int_{\max(\tau_{\text{form}},\tau_i)}^{\tau_f} d\tau\,\Gamma(p_T,\mathbf{x}_\perp,\Theta). \tag{37}$$

Here, τ_{form} is the formation time of the particular state in the laboratory frame and τ_f is the time when the hard momentum scale reaches T_c. To study the nuclear suppression of a particular state, one needs to take into account the decay of the excited states to this particular state (so-called feed down). For RHIC energies, using the value of $dN_{\text{ch}}/dy = 620$ and various values of η/S (note that η/S is related to the anisotropy parameter, ξ) the corresponding initial temperatures are estimated with $\tau_i = 0.3$ fm/c. p_T integrated R_{AA} values of individual bottomonium states (direct production) have been calculated using both the potentials A and B [56, 57] as functions of number of participants and rapidity. It is seen that for both potentials, more suppression is observed in case of anisotropic medium than in the isotropic case. However, the suppression is more in case of potential model A. There is also indication of sequential suppression [56, 57]. Similar exercise has also been done in case of LHC energies ($\sqrt{s} = 2.76$ TeV) using a constant value of η/S. It is again observed that the suppression in case of potential A is more. These findings can be used to constrain η/S by comparing with the RHIC and LHC data.

Next, we discuss the effect of the initial state momentum anisotropy on the survival probability of J/ψ due to gluon dissociation. This is important as we have to take into account all possibilities of quarkonium getting destroyed in the QGP to estimate the survival probability and hence R_{AA}. In contrast to Debye screening, this is another possible mechanism of J/ψ suppression in QGP. In QGP, the gluons have much harder momentum, sufficient to dissociate the charmonium.

Such a study was performed in an isotropic plasma [58]. In this context, we will study the thermally weighted gluon dissociation cross of J/ψ in an anisotropic media.

Bhanot and Peskin first calculated the quarkonium-hadron interaction cross-section using operator product expansion [59]. The perturbative prediction for the gluon J/ψ dissociation cross-section is given by [60]

$$\sigma\left(q^0\right) = \frac{2\pi}{3}\left(\frac{32}{3}\right)^2\left(\frac{16\pi}{3g_2}\right)\frac{1}{m_Q^2}\frac{\left(q^0/\epsilon_0 - 1\right)^{3/2}}{\left(q^0/\epsilon_0\right)^5}, \quad (38)$$

where q^0 is the energy of the gluon in the stationary J/ψ frame; ϵ_0 is the binding energy of the J/ψ where $q_0 > \epsilon_0$, and m_Q is charm quark mass. It is to be noted that we have used the constant binding energy of the J/ψ in AQGP at finite temperature. We assume that the J/ψ moves with four momentum P given by

$$P = \left(M_T \cosh y, 0, P_T, M_T \sinh y\right), \quad (39)$$

where $M_T = \sqrt{M_{J/\psi}^2 + P_T^2}$ is the J/ψ transverse mass and y is the rapidity of the J/ψ. A gluon with a four momentum $K = (k^0, \mathbf{k})$ in the rest frame of the parton gas has energy $q^0 = K \cdot u$ in the rest frame of the J/ψ. The thermal gluon J/ψ dissociation cross-section in anisotropic media is defined as [15, 58]

$$\left\langle \sigma\left(K \cdot u\right) v_{\text{rel}} \right\rangle_k = \frac{\int d^3k \sigma\left(K \cdot u\right) v_{\text{rel}} f\left(k^0, \xi, p_{\text{hard}}\right)}{\int d^3k f\left(k^0, \xi, p_{\text{hard}}\right)}, \quad (40)$$

where $v_{\text{rel}} = 1 - (\mathbf{k} \cdot \mathbf{P})/(k^0 M_T \cosh y)$ is the relative velocity between J/ψ and the gluon. Now changing the variable ($K \leftrightarrow Q$), one can obtain by using Lorentz transformation [15], the following relations:

$$k^0 = \frac{\left(q^0 E + q\left(\sin\theta_p \sin\theta_q \sin\phi_q + \cos\theta_p \cos\theta_q\right)\right)}{M_{J/\psi}},$$

$$\mathbf{k} = \mathbf{q} + \frac{qE}{|\mathbf{P}| M_{J/\psi}} \times \left[\left(qM_T \cosh y - M_{J/\psi}\right) \times \left(\sin\theta_p \sin\theta_q \sin\phi_q + \cos\theta_p \cos\theta_q\right) + |\mathbf{P}|\right] \mathbf{v}_{\mathbf{J/\psi}}, \quad (41)$$

where $\mathbf{v}_{\mathbf{J/\psi}} = \mathbf{P}/E$, $P = (E, 0, |\mathbf{P}| \sin\theta_p, |\mathbf{P}| \cos\theta_p)$, and $\mathbf{q} = (q \sin\theta_q \cos\phi_q, q \sin\theta_q \sin\phi_q, q \cos\theta_q)$. In the rest frame of J/ψ, numerator of (40) can be written as

$$\int d^3q \frac{M_{J/\psi}}{E} \sigma\left(q^0\right) f\left(k^0, \xi, p_{\text{hard}}\right), \quad (42)$$

while, the denominator of (40) can be written as [30]

$$\int d^3k f\left(k^0, \xi, p_{\text{hard}}\right) = \int d^3k f_{\text{iso}}\left(\sqrt{\mathbf{k}^2 + \xi(\mathbf{k} \cdot \hat{\mathbf{n}})^2}, p_{\text{hard}}\right) = \frac{1}{\sqrt{1+\xi}} 8\pi\zeta(3) p_{\text{hard}}^3, \quad (43)$$

where $\zeta(3)$ is the Riemann zeta function. The maximum value of the gluon J/ψ dissociation cross-section [60] is about 3 mb in the range $0.7 \leq q^0 \leq 1.7$ GeV. Therefore high-momentum gluons do not see the large object and simply passes through it, and the low-momentum gluons cannot resolve the compact object and cannot raise the constituents to the continuum.

To calculate the survival probability of J/ψ in an anisotropic plasma, we consider only the longitudinal expansion of the matter. The survival probability of the J/ψ in the deconfined quark-gluon plasma is

$$S\left(P_T\right) = \frac{\int d^2r \left(R_A^2 - r^2\right) \exp\left[-\int_{\tau_i}^{\tau_{\max}} d\tau\, n_g(\tau) \left\langle \sigma\left(K \cdot u\right) v_{\text{rel}} \right\rangle_k\right]}{\int d^2r \left(R_A^2 - r^2\right)}, \quad (44)$$

where $\tau_{\max} = \min(\tau_\psi, \tau_f)$ and τ_i are the QGP formation time. $n_g(\tau) = 16\zeta(3) p_{\text{hard}}^3(\tau)/[\pi^2\sqrt{1+\xi(\tau)}]$ is the gluon density at a given time τ. Now the J/ψ will travel a distance in the transverse direction with velocity $\mathbf{v}_{J/\psi}$ given by

$$d = -r\cos\phi + \sqrt{R_A^2 - r^2\left(1 - \cos^2\phi\right)}, \quad (45)$$

where $\cos\phi = \hat{v}_{J/\psi} \cdot \hat{r}$. The time interval $\tau_\psi = M_T d/P_T$ is the time before J/ψ escapes from a gluon gas of transverse extension $R_\perp$. The time evaluation of ξ and p_{hard} is determined by (3) and (4).

We now first discuss the numerical result of the thermal averaged gluon dissociation cross-section in the anisotropic system. The results are displayed in Figure 4 for $P_T = 0$ and $P_T = 8$ GeV for a set of values of the anisotropy parameter. It is seen that the velocity averaged cross-section decreases with ξ for p_{hard} up to ~500 MeV and then increases as compared to the isotropic case ($\xi = 0$) (see Figure 4(a)). For higher P_T, a similar feature has been observed in Figure 4(b), where the cross-section starts to increase beyond $p_{\text{hard}} \sim 200$ MeV. For fixed p_{hard}, the dissociation cross-section as a function of P_T shows that the cross-section first decreases and then marginally increases [15].

Equation (44) has been used to calculate the survival probability. Figure 5 describes the survival probability of J/ψ for various values of the isotropization time τ_{iso} at RHIC energy. Left (Right) panel corresponds to $\theta_p = \pi/2$ ($\theta_p = \pi/3$). It is observed that the survival probability remains the same as in the isotropic case upto $P_T = 4$ GeV in the central region. Beyond that marginal increase is observed with the increase of τ_{iso}. In the forward rapidity, the results are almost the same as the isotropic case throughout the whole P_T region. For this set of initial conditions, the argument of the exponential in (44) becomes similar to that of the isotropic case. Also the dissociation cross-section first decreases with P_T and then increases. Because of these reasons, we observe minor change in the survival probability [15]. Therefore, the survival probability is more or less independent of the direction of propagation of the J/ψ with respect to the anisotropy axis, whereas in the case of radiative energy loss of

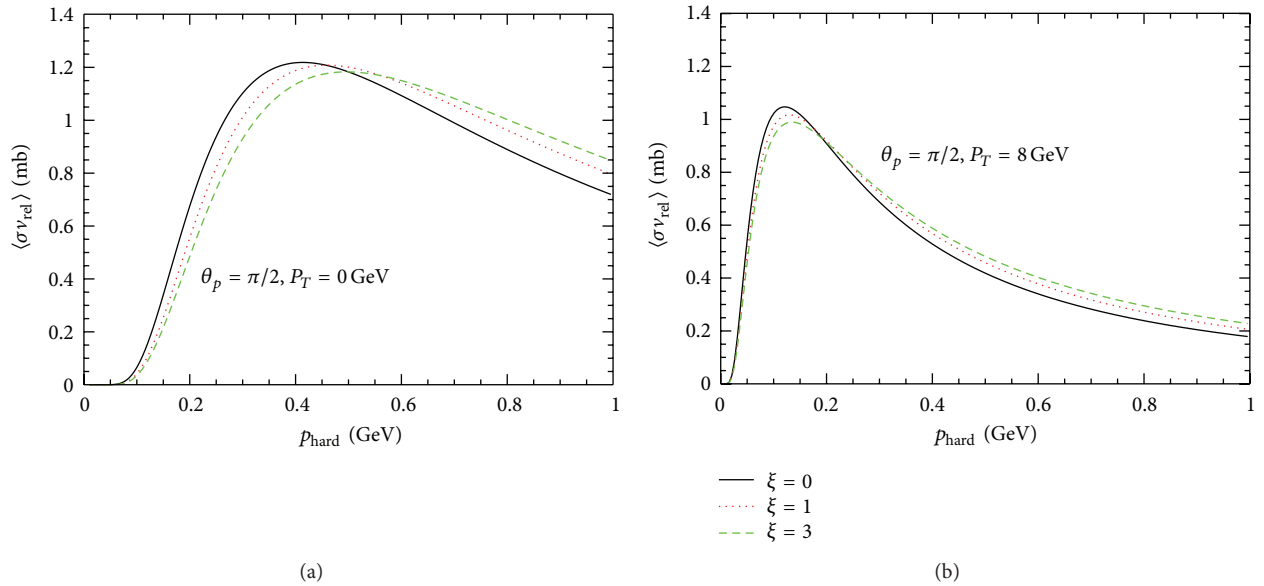

FIGURE 4: (Color online) The thermal-averaged gluon J/ψ dissociation cross-section as function of the hard momentum scale at central rapidity ($\theta_p = \pi/2$) for $\xi = \{0, 1, 3, 5\}$. (a) corresponds to $P_T = 0$ and (b) is for $P_T = 8$ GeV.

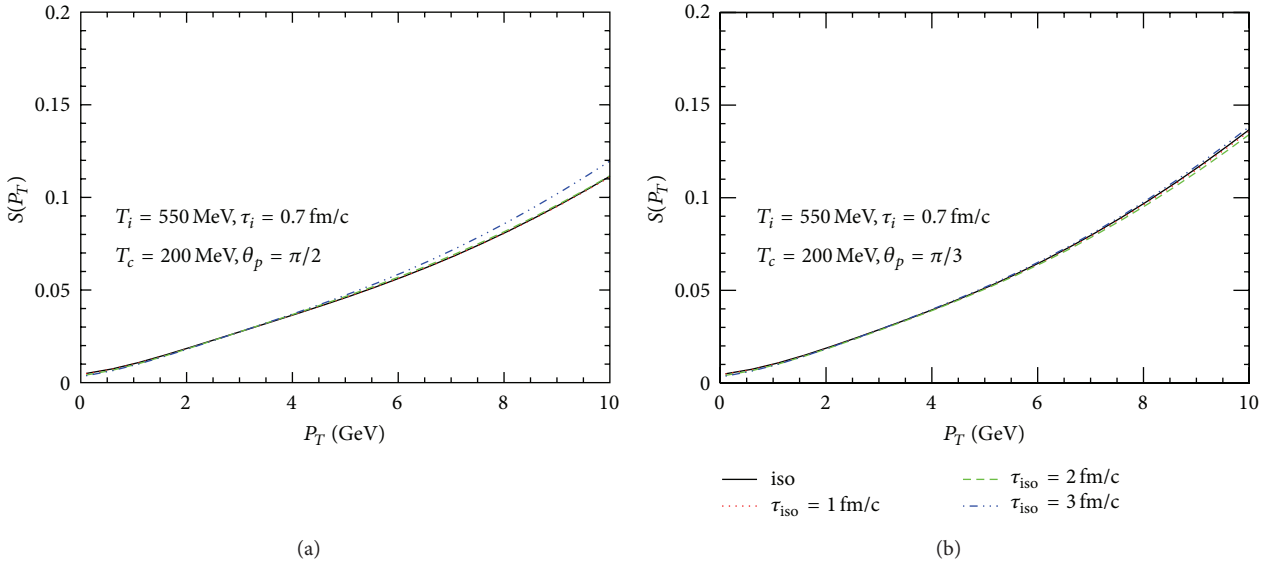

FIGURE 5: (Color online) The survival probability of J/ψ in an anisotropic plasma at central and forward rapidity region. The initial conditions are taken as $T_i = 550$ MeV, $T_c = 200$ MeV, and $\tau_i = 0.7$ fm/c.

fast partons in anisotropic media the result has been shown to depend strongly on the direction of propagation [32]. The results for the LHC energies for the two sets of initial conditions at two values of the transition temperatures are shown in Figure 6. For set I, we observe marginal increase as in the case for set I at RHIC energies. However, for set II substantial modification is observed for the reason stated earlier.

4. Radiative Energy Loss and R_{AA} of Light Hadrons

In this section, we calculate the radiative energy loss in an infinitely extended anisotropic plasma. We assume that an on-shell quark produced in the remote past is propagating through an infinite QCD medium that consists of randomly distributed static scattering centers which provide a color-screened Yukawa potential originally developed for the isotropic QCD medium given by [61]

$$V_n = V(q_n) e^{i\mathbf{q}_n \cdot \mathbf{x}_n} = 2\pi\delta(q^0)\, v(q_n)\, e^{-i\mathbf{q}_n \cdot \mathbf{x}_n} T_{a_n}(R) \otimes T_{a_n}(n), \quad (46)$$

with $v(\mathbf{q}_n) = 4\pi\alpha_s/(q_n^2 + m_D^2)$. x_n is the location of the nth scattering center, T denotes the color matrices of the parton and the scattering center. It is to be noted that the

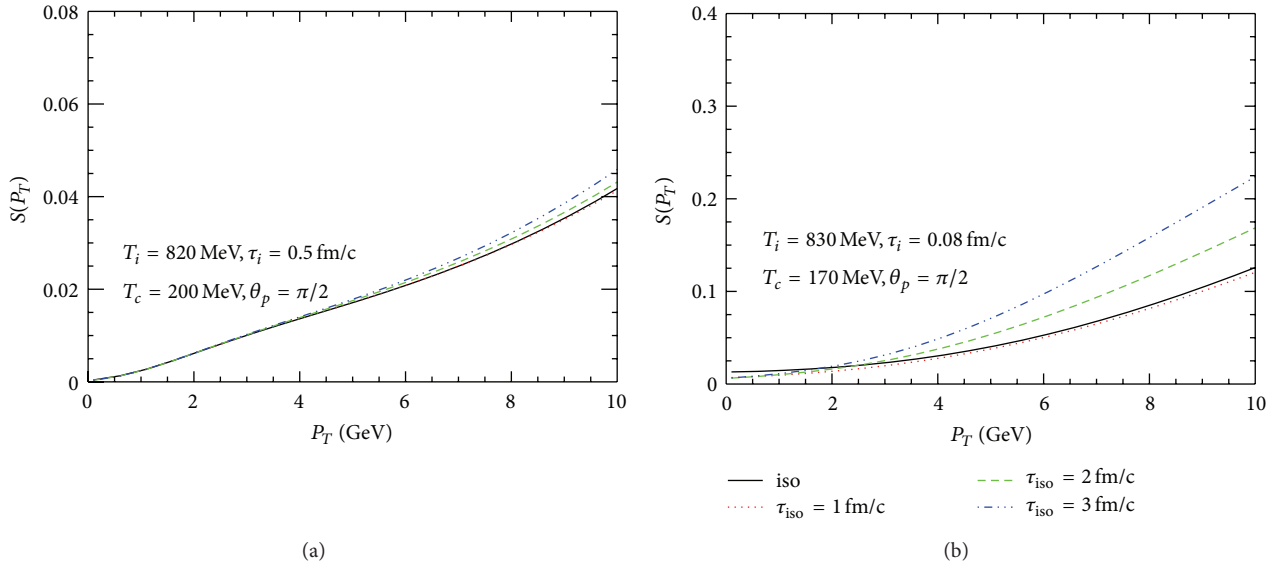

FIGURE 6: (Color online) The survival probability of J/ψ in an anisotropic plasma for the two sets of initial conditions at LHC energies. Left (right) panel corresponds to T_c = 200(170) MeV.

potential has been derived by using hard thermal loop (HTL) propagator in QGP medium. In anisotropic plasma, the two-body interaction, as expected, becomes direction dependent. The two-body potential required to calculate the radiative energy loss has been calculated in the previous section.

Now the parton scatters with one of the color center with the momentum $Q = (0, q_\perp, q_z)$ and subsequently radiates a gluon with momentum $K = (\omega, k_\perp, k_z)$. The quark energy loss is calculated by folding the rate of gluon radiation $\Gamma(E)$ with the gluon energy by assuming $\omega + q_0 \approx \omega$. In the soft-scattering approximation, one can find the quark radiative energy loss per unit length as [62]

$$\frac{dE}{dL} = \frac{E}{D_R}\int x\,dx\frac{d\Gamma}{dx}. \tag{47}$$

Here, D_R is defined as $[t_a, t_c][t_c, t_a] = C_2(G)C_R D_R$, where $C_2(G) = 3$, $D_R = 3$, and $C_R = 4/3$. x is the longitudinal momentum fraction of the quark carried away by the emitted gluon.

Now in anisotropic medium we have [32]

$$x\frac{d\Gamma}{dx} = \frac{C_R\alpha_s}{\pi}\frac{L}{\lambda}\frac{m_D^2}{16\pi^2\alpha_s} \times \int \frac{d^2k_\perp}{\pi}\frac{d^2q_\perp}{\pi}\left|V(q_\perp, q_z, \xi)\right|^2 \times \left[\frac{k_\perp + q_\perp}{(k_\perp + q_\perp)^2 + \chi} - \frac{k_\perp}{k_\perp^2 + \chi}\right]^2, \tag{48}$$

where $\chi = m_q^2 x^2 + m_g^2$ with $m_g^2 = m_D^2/2$ and $m_q^2 = m_D^2/6$, and $V(q_\perp, q_z, \xi)$ is given by (26).

In the present scenario, we assume that the parton is propagating along the z direction and makes an angle θ_n with the anisotropy direction. In such case, we replace $q_\perp$ and q_z in (26) by $q_\perp \to \sqrt{q_\perp^2 - q_\perp^2 \sin^2\theta_n \cos^2\phi}$ and $q_z \to |\mathbf{q}| \sin\theta_n \cos\phi$. For arbitrary ξ the radiative energy loss can be written as [32]

$$\begin{aligned}\frac{\Delta E}{E} &= \frac{C_R\alpha_s}{\pi^2}\frac{Lm_D^2}{\lambda} \times \int dx\,d^2q_\perp \frac{\left|V(q_\perp, q_z, \xi)\right|^2}{16\pi^2\alpha_s^2} \times \left[-\frac{1}{2} - \frac{k_m^2}{k_m^2 + \chi} + \frac{q_\perp^2 - k_m^2 + \chi}{2\sqrt{q_\perp^4 + 2q_\perp^2(\chi - k_m^2)} + (k_m^2 + \chi)^2} + \frac{q_\perp^2 + 2\chi}{q_\perp^2\sqrt{1 + 4\chi/q_\perp^2}} \times \ln\left(\frac{k_m^2 + \chi}{\chi} \times \left(\left(\left(q_\perp^2 + 3\chi\right) + \sqrt{1 + 4\chi/q_\perp^2}\left(q_\perp^2 + \chi\right)\right) \times \left(\left(q_\perp^2 - k_m^2 + 3\chi\right) + \sqrt{1 + 4\chi/q_\perp^2} \times \sqrt{q_\perp^4 + 2q_\perp^2(\chi - k_m^2)} + \left(k_m^2 + \chi\right)^2\right)^{-1}\right)\right)\right].\end{aligned} \tag{49}$$

In the previous expression, λ denotes the average mean-free path of the quark scattering and is given by

$$\frac{1}{\lambda} = \frac{1}{\lambda_g} + \frac{1}{\lambda_q}, \tag{50}$$

which depends on the strength of the anisotropy. In the last expression λ_q and λ_g correspond to the contributions coming from q-q and q-g scattering, respectively. Consider

$$\frac{1}{\lambda_i} = \frac{C_R C_2(i)\,\rho(i)}{N_c^2 - 1} \int \frac{d^2 q_\perp}{(2\pi)^2} \left|V(q_\perp, 0, \xi)\right|^2, \tag{51}$$

where $C_2(i)$ is the Cashimir for the d_i-dimensional representation and $C_2(i) = (N_c^2 - 1)/(2N_c)$ for quark and $C_2(i) = N_c$ for gluon scatterers. ρ_i is the density of the scatterers. Using $\rho_i = \rho_i^{\text{iso}} \sqrt{1+\xi}$, we obtain

$$\frac{1}{\lambda} = \frac{18\alpha_s p_{\text{hard}} \zeta(3)}{\pi^2 \sqrt{1+\xi}} \frac{1}{R(\xi)} \frac{1 + N_F/6}{1 + N_F/4}, \tag{52}$$

where N_F is the numbers of flavors.

The fractional energy loss in anisotropy medium for the light quark is shown in Figure 7. We consider a plasma at a temperature $T = 250$ MeV with the effective number of degrees of freedom $N_F = 2.5$, $\alpha_s = 0.3$ and the length of the medium is $L = 5$ fm. The energy loss in the anisotropic media depends on the angle of propagation of the fast parton with respect to the anisotropy axis ($\hat{\mathbf{n}}$). We see that the fractional energy loss increases in the direction parallel to the anisotropy axis. With the increase of anisotropy parameter ξ the fractional energy loss subsequently increases for $\theta_n = \pi/6$. However, away from the anisotropy axis ($\theta_n = \pi/2$), the fractional energy loss decreases because the quark-quark potential is stronger in the anisotropy direction [32]. In the perpendicular direction to the anisotropy axis, the fractional energy loss is quite small. The fractional energy loss for the heavy quarks (i.e., for charm and bottom) is shown in Figure 8. The fractional energy loss is enhanced in the direction parallel to anisotropy axis as well as for $\theta_n = \pi/6$. However, for $\theta_n = \pi/2$, the fractional energy loss decreases for both heavy and light quarks.

Next, we consider the nuclear modification factor of light hadrons incorporating the light quark energy loss in AQGP discussed in the previous paragraphs. When a parton is propagating in the direction of anisotropy it is found that the fractional energy loss increases. In this section, we will apply this formalism to calculate the nuclear modification factor of the light hadrons. Starting with two-body scattering at the parton level, the differential cross-section for the hadron production is [63]

$$E\frac{d\sigma}{d^3p}(AB \longrightarrow \text{jet} + X) = K \sum_{abcd} \int dx_a dx_b G_{a/h_A}(x_a, Q^2)\, G_{b/h_B} \times (x_b, Q^2)\, \frac{\hat{s}}{\pi} \frac{d\sigma}{d\hat{t}} (ab \longrightarrow cd)\, \delta(\hat{s} + \hat{t} + \hat{u}). \tag{53}$$

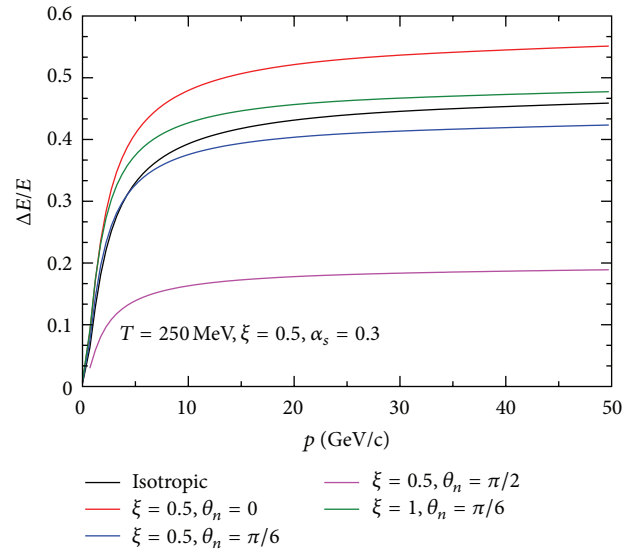

FIGURE 7: Color online: fractional energy loss for the light quark for $\xi = (0.5, 1)$.

The argument of the δ function can be expressed in terms of x_a and x_b, and doing the x_b integration we arrive at the final expression as follows:

$$E\frac{d\sigma}{d^3p}(AB \longrightarrow \text{jet} + X) = K \sum_{abcd} \int_{x_{\min}}^{1} dx_a G_{a/h_A}(x_a, Q^2)\, G_{b/h_B} \times (x_b, Q^2)\, \frac{2}{\pi} \frac{x_a x_b}{2x_a - x_T e^y} \frac{d\sigma}{d\hat{t}} (ab \longrightarrow cd), \tag{54}$$

where $x_b = (x_a x_T e^{-y})/(2x_a - x_T e^y)$, $x_T = 2p_T/\sqrt{s}$, and $x_{\min} = x_T e^y/(2 - x_T e^{-y})$, and the factor K is introduced to take into account the higher-order effects. It should be noted that to obtain single-particle inclusive invariant cross-section, the fragmentation function $D_{h/c}(z, Q^2)$ must be included. To obtain the hadronic p_T spectra in A-A collisions, we multiply the result by the nuclear overlap function for a given centrality. The inclusion of jet quenching as a final state effect in nucleus-nucleus collisions can be implemented in two ways: (i) modifying the partonic p_T spectra [64] and (ii) modifying the fragmentation function [65] but keeping the partonic p_T spectra unchanged. In this calculation we intend to modify the fragmentation function. The effective fragmentation function can be written as

$$D_{h/c}(z, Q^2) = \frac{z^*}{z} D_{h/c}(z^*, Q^2), \tag{55}$$

where $z^* = z/(1 - \Delta E/E)$ is the modified momentum fraction. Now we take into account the jet production geometry. We assume that all the jets are not produced at the same point; therefore, the path length transversed by the partons before

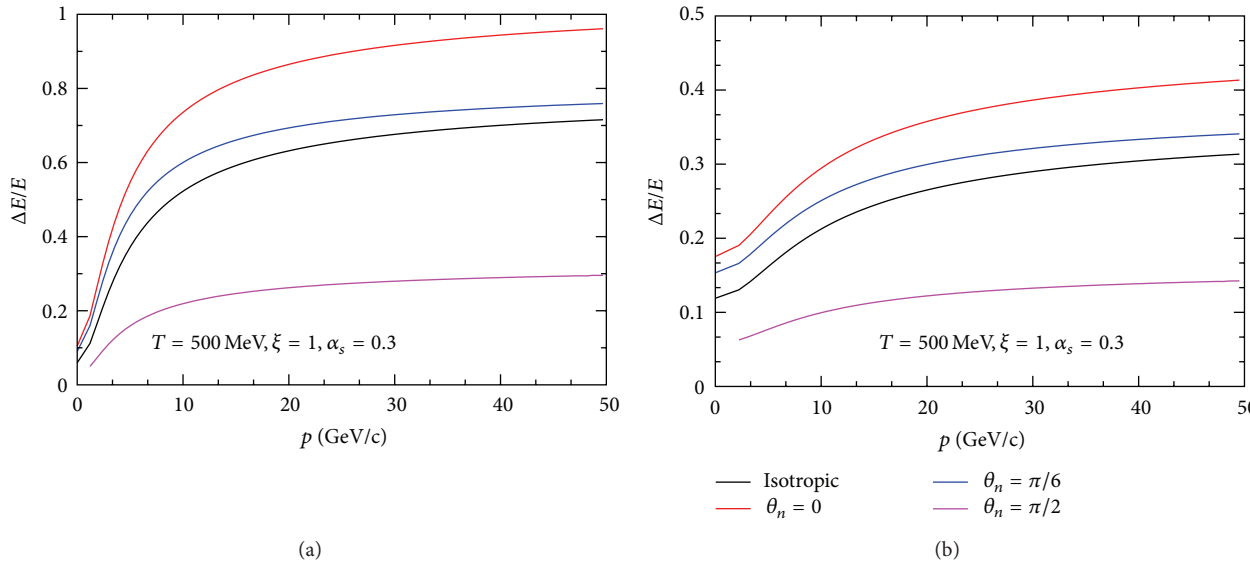

FIGURE 8: (Color online) Same as 7 for charm quark (a) and bottom quark (b) with $\xi = 1$ and $T = 500$ MeV.

the fragmentation is not the same. We consider a jet initially produced at (r, ϕ) and leaves the plasma after a proper time (t_L) or equivalently after traversing a distance L (for light quarks $t_L = L$) where

$$L(r,\phi) = \sqrt{R_\perp^2 - r^2 \sin\phi^2} - R_\perp \cos\phi, \tag{56}$$

where $R_\perp$ is the transverse dimension of the system. Since the number of jets produced at $\mathbf{r}$ is proportional to the number of binary collisions, the probability is proportional to the product of the thickness functions as follows:

$$\mathscr{P}(\vec{r}) \propto T_A(\vec{r})\, T_B(\vec{r}). \tag{57}$$

In case of hard sphere $\mathscr{P}(r)$ is given by [66]

$$\mathscr{P}(r) = \frac{2}{\pi R_\perp^2}\left(1 - \frac{r^2}{R_\perp^2}\right)\theta(R_\perp - r), \tag{58}$$

where $\int d^2r\, \mathscr{P}(r) = 1$. To obtain the hadron p_T spectra, we have to convolute the resulting expression over all transverse positions and the expression is

$$\frac{dN^{\pi^0(\eta)}}{d^2p_T dy} = \sum_f \int d^2r \mathscr{P}(r) \int_{t_i}^{t_L} \frac{dt}{t_L - t_i} \times \int \frac{dz}{z^2} D_{\pi^0(\eta)/f}\left(z, Q^2\right)\Big|_{z=p_T/p_T^f} E\frac{dN}{d^3p^f}. \tag{59}$$

The quantity $E(dN/d^3p^f)$ is the initial momentum distribution of jets and can be computed using LO-pQCD. Here, we use average distance traversed by the partons, $\langle L\rangle$ is given by

$$\langle L\rangle = \frac{\int_0^{R_T} r dr \int_0^{2\pi} L(\phi, r)\, T_{AA}(r, b=0)\, d\phi}{\int_0^{R_T} r dr \int_0^{2\pi} T_{AA}(r, b=0)\, d\phi}, \tag{60}$$

where $\langle L\rangle \sim 5.8(6.2)$ fm for RHIC (LHC). Finally, the nuclear modification factor (R_{AA}) becomes [44]

$$R_{AA}(p_T) = \frac{dN_{AA}^{\pi^0(\eta)}/d^2p_T dy}{\left[dN_{AA}^{\pi^0(\eta)}/d^2p_T dy\right]_0}, \tag{61}$$

where $[dN_{AA}^{\pi^0(\eta)}/d^2p_T dy]_0$ corresponds to the hadron p_T distribution without the energy loss.

For an expanding plasma, the anisotropy parameter p_{hard} and ξ are time dependent. The time evaluation is again given by (3) and (4). In the present work, it is assumed that an isotropic QGP is formed at an initial time τ_i and initial temperature T_i. Rapid longitudinal expansion of the plasma leads to an anisotropic QGP which lasts till τ_{iso}. For 0–10% centrality (relevant for our case), we obtain $T_i = 440(350)$ MeV for $\tau_i = 0.147(0.24)$ fm/c. at RHIC energy [44].

Figure 9 describes the nuclear modification factor for two different initial conditions with various values of isotropization time, τ_{iso} along with the PHENIX data [67]. It is quite clear from Figure 9(a) that the value of R_{AA} for anisotropic medium is lower than that for the isotropic media as the energy loss in the anisotropy medium is higher [32]. It is also observed that as τ_{iso} increases the value of R_{AA} decreases compared to its isotropic value [44]. This is because the hard scale decreases slowly as compared to the isotropic case, that is, the cooling is slow. For reasonable choices of τ_{iso}, the experimental data is well described. It is seen that increasing the value of τ_{iso} beyond 1.5 fm/c grossly underpredict the data. We find that the extracted value of isotropization time lies in the range $0.5 \le \tau_{\text{iso}} \le 1.5$ fm/c [44]. This is in agreement with the earlier finding of τ_{iso} using PHENIX photon data [16]. In order to see the sensitivity on the initial conditions we now consider another set of initial conditions, $T_i = 350$ MeV and $\tau_i = 0.24$ fm/c. The result is shown in Figure 9(b). It is observed that to reproduce the data a larger value of τ_{iso} is

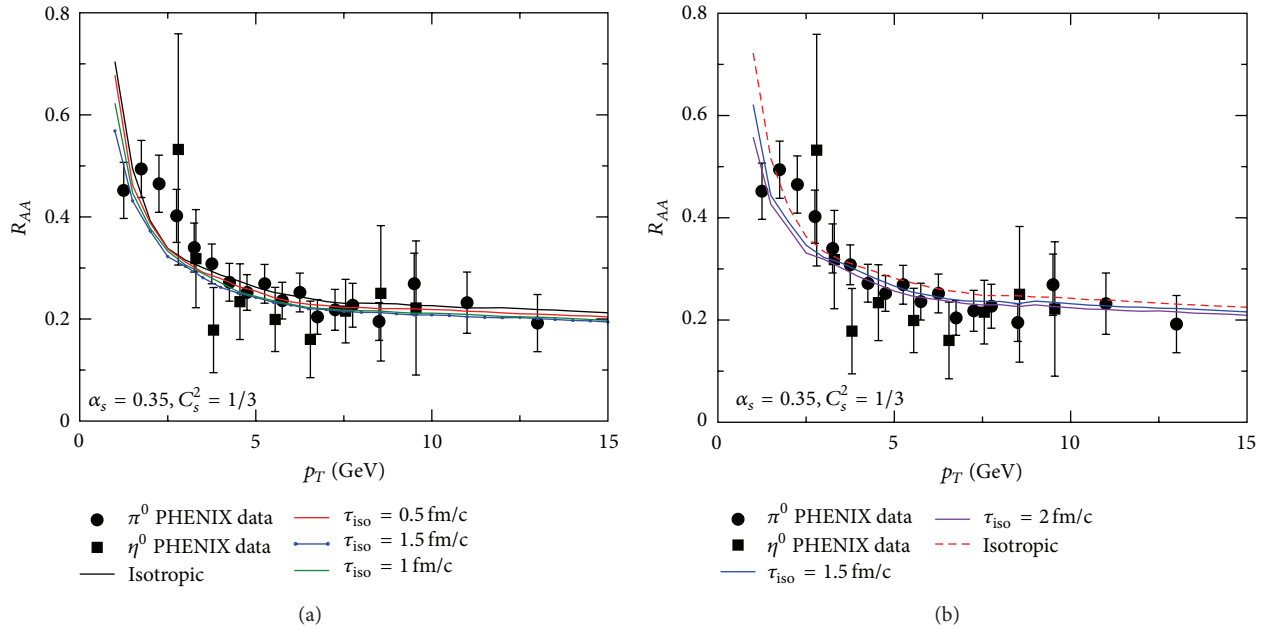

FIGURE 9: (Color Online) Nuclear modification factor at RHIC energies. The initial conditions are taken as (a) $T_i = 440$ MeV and $\tau_i = 0.147$ fm/c and (b) $T_i = 350$ MeV and $\tau_i = 0.24$ fm/c.

needed as compared to the case of higher initial temperature. We extract an upper limit of $\tau_{iso} = 2$ fm/c [44] in this case.

5. Plasma Wakes

It is mentioned earlier that when a jet propagates through hot and dense medium it loses energy mainly by the radiative process. As mentioned earlier, it also creates wake in the charge density as well as in the potential. Now, we calculate the wake in charge density and the wake potential due to the passage of a fast parton in a small ξ limit. Dielectric function contains essentially all the information of the chromoelectromagnetic properties of the plasma. The dielectric function $\epsilon(\mathbf{k}, \omega)$ can be calculated from the dielectric tensor using the following relation:

$$\epsilon(\mathbf{k}, \omega) = \frac{k_i \epsilon^{ij}(\mathbf{k}, \omega) k_j}{k^2}, \tag{62}$$

where the dielectric tensor ϵ^{ij} can be written in terms of the gluon polarization tensor as follows (given by (18)):

$$\epsilon^{ij} = \delta^{ij} - \frac{\Pi^{ij}}{\omega^2}. \tag{63}$$

Therefore, the dielectric function is directly related to the structure functions mentioned in Section 3 through (18), (63), and (62). To get the analytic expressions for the structure functions, one must resort to small ξ limit. To linear order in ξ, we have [28]

$$\begin{aligned}
\alpha &= \Pi_T(z) \\
&\quad + \xi \left[\frac{z^2}{12}(3 + 5\cos 2\theta_n) m_D^2 - \frac{1}{6}(1 + \cos 2\theta_n) m_D^2 \right. \\
&\quad \left. + \frac{1}{4}\Pi_T(z)\left((1 + 3\cos 2\theta_n) - z^2(3 + 5\cos 2\theta_n)\right) \right], \\
\beta &= z^2 \left[\Pi_L(z) \right. \\
&\quad + \xi \left[\frac{1}{6}(1 + 3\cos 2\theta_n) m_D^2 \right. \\
&\quad \left. \left. + \Pi_L(z)\left(\cos 2\theta_n - \frac{z^2}{2}(1 + 3\cos 2\theta_n)\right) \right] \right], \\
\gamma &= \frac{\xi}{3}\left(3\Pi_T(z) - m_D^2\right)\left(z^2 - 1\right)\sin^2\theta_n, \\
\delta &= \frac{\xi}{3k}\left[4z^2 m_D^2 + 3\Pi_T(z)\left(1 - 4z^2\right)\right]\cos\theta_n,
\end{aligned} \tag{64}$$

with

$$\begin{aligned}
\Pi_T(K) &= \frac{m_D^2}{2} z^2 \\
&\quad \times \left[1 - \frac{1}{2}\left(z - \frac{1}{z}\right)\left(\ln\left|\frac{z+1}{z-1}\right| - i\pi\Theta\left(1 - z^2\right)\right)\right], \\
\Pi_L(K) &= m_D^2 \left[\frac{z}{2}\left(\ln\left|\frac{z+1}{z-1}\right| - i\pi\Theta\left(1 - z^2\right)\right) - 1\right],
\end{aligned} \tag{65}$$

where $z = \omega/k$.

In the presence of the test charge particle, the induced charge density and the wake potential depend on the velocity of the external charged parton and also on the distribution

of the background particle [68]. When a static test charge is introduced in a plasma, it acquires a shielding cloud. As a result, the induced charge distribution is spherically symmetric. When a charge particle is in motion relative to the plasma, the induced charge distribution no longer remains symmetric. As a result spherical symmetry of the screening cloud reduces to ellipsoidal shape.

The passage of external test charge through the plasma also disturbs the plasma and creates induced color charge density [69]. Therefore, the total color charge density is given as

$$\rho^a_{\text{tot}}(\mathbf{k},\omega) = \rho^a_{\text{ext}}(\mathbf{k},\omega) + \rho^a_{\text{ind}}(\mathbf{k},\omega), \tag{66}$$

where a represents the color index. However, the total color charge density is linearly related to ρ^a_{ext} through the dielectric response function ($\rho^a_{\text{tot}}(\mathbf{k},\omega) = \rho^a_{\text{ext}}(\mathbf{k},\omega)/\epsilon(\mathbf{k},\omega)$). Therefore, the induced color charge density is explicitly written as

$$\rho^a_{\text{ind}}(\mathbf{k},\omega) = \left(\frac{1}{\epsilon(\mathbf{k},\omega)} - 1\right)\rho^a_{\text{ext}}(\mathbf{k},\omega). \tag{67}$$

Now, we consider a charge particle Q^a moving with a constant velocity $\mathbf{v}$ and interacting with the anisotropic plasma. The external charge density associated with the test charge particle can be written as [33, 34, 38]

$$\rho^a_{\text{ext}} = 2\pi Q^a \delta(\omega - \mathbf{k}\cdot\mathbf{v}). \tag{68}$$

The delta function indicates that the value of ω is real and the velocity of the charge particle is restricted between $0 < v < 1$, which is known as the Cerenkov condition for the moving parton in the medium. Therefore, the collective modes are determined in the space-like region of the ω-k plane [34, 38]. According to Cerenkov condition, there will be two important scenarios which occur due to the interaction of the particle and the plasmon wave: first, the modes which are moving with a speed less than the average speed of the plasmon modes can be excited, but the particle moving slightly slower than the wave will be accelerated. While the charge particle moving faster than the wave will decrease its average velocity [69]. The slowly moving particle absorbs energy from the wave, the faster moving particle transfers its extra energy to the wave. The absorption and emission of energy result in a wake in the induced charge density as well as in the potential. Second, when the charge particle moving with a speed greater than the average phase velocity v_p, the modes are excited and they may not be damped. Such excited modes can generate Cerenkov-like radiation and a Mach stem [70] which leads to oscillation both in the induced charge density and in the wake potential.

Substituting (68) into (67) and transforming into $\mathbf{r}$-t space, the induced charge density becomes

$$\begin{aligned}\rho^a_{\text{ind}}(\mathbf{r},t) = {} & 2\pi Q^a \int \frac{d^3k}{(2\pi)^3} \\ & \times \int \frac{d\omega}{2\pi} \exp^{i(\mathbf{k}\cdot\mathbf{r}-\omega t)} \left(\frac{1}{\epsilon(\mathbf{k},\omega)} - 1\right) \\ & \times \delta(\omega - \mathbf{k}\cdot\mathbf{v}).\end{aligned} \tag{69}$$

First, we consider the case where the fast parton is moving in the beam direction, that is, $\mathbf{v} \parallel \hat{\mathbf{n}}$. In spherical coordinate system $\mathbf{k} = (k\sin\theta_n\cos\phi, k\sin\theta_n\sin\phi, k\cos\theta_n)$ and the cylindrical coordinate for $\mathbf{r} = (\rho, 0, z)$; therefore, the induced charge density can be written as

$$\begin{aligned}\rho^a_{\text{ind}}(\mathbf{r},t) = {} & \frac{Q^a m_D^3}{2\pi^2} \int_0^\infty dk\, k^2 \\ & \times \int_0^1 d\chi\, J_0\left(k\rho\sqrt{1-\chi^2}m_D\right) \\ & \times \left[\cos\Gamma\left(\frac{\text{Re}\,\epsilon(\mathbf{k},\omega)}{\Delta} - 1\right)\right. \\ & \left. + \sin\Gamma\frac{\text{Im}\,\epsilon(\mathbf{k},\omega)}{\Delta}\right]\Bigg|_{\omega=\mathbf{k}\cdot\mathbf{v}},\end{aligned} \tag{70}$$

where χ is represented as $\cos\theta_n$, J_0 is the zeroth-order Bessel function, $\Gamma = k\chi(z - vt)m_D$, and $\Delta = (\text{Re}\,\epsilon(\mathbf{k},\omega))^2 + (\text{Im}\,\epsilon(\mathbf{k},\omega))^2$. To get the previous equation, we use the simple transformation $\omega \to \omega m_D$ and $k \to k m_D$. It is seen that the charge density ρ^a_{ind} is proportional to m_D^3.

Numerical evaluation of the previous equation leads to the contour plots of the induced charge density shown in Figure 10 with two different speeds of the fast parton. The contour plot of the equicharge lines shows a sign flip along the direction of the moving parton in Figure 10. The left (right) panel shows the contour plot of the induced color charge density in both isotropic and anisotropic plasma with parton velocity $v = 0.55(0.99)$. It is clearly seen that, because of anisotropy, the positive charge lines appear alternately in the backward space which indicates a small oscillatory behavior of the color charge wake (see Figure 10(c)). When the charge particle moves faster than the average plasmon speed, the induced charge density forms a cone-like structure which is significantly different from when the parton velocity is $v = 0.55$. It is also seen that the induced charge density is oscillatory in nature. The supersonic nature of the parton leads to the formation of Mach cone and the plasmon modes could emit a Cerenkov-like radiation, which spatially limits the disturbances in the induced charge density [71]. In the backward space ($(z - vt) < 0$), induced color charge density is very much sensitive to the anisotropic plasma than that in the forward space ($(z - vt) > 0$). Due to the effect of the anisotropy, the color charge wake is modified significantly and the oscillatory behavior is more pronounced than the isotropic case. It is also seen that the oscillatory nature increases with the increase of the anisotropic parameter ξ.

Next, we consider the case when the parton moves perpendicular to the anisotropy direction in which case the induced charge density can be written as

$$\begin{aligned}\rho^a_{\text{ind}}(\mathbf{r},t) = {} & \frac{Q^a m_D^3}{2\pi^2} \int_0^\infty dk\, k^2 \\ & \times \int_0^1 d\chi \int_0^{2\pi} \frac{d\phi}{2\pi} \left[\cos\Omega\left(\frac{\text{Re}\,\epsilon(\mathbf{k},\omega)}{\Delta} - 1\right)\right. \\ & \left. + \sin\Omega\frac{\text{Im}\,\epsilon(\mathbf{k},\omega)}{\Delta}\right]\Bigg|_{\omega=\mathbf{k}\cdot\mathbf{v}},\end{aligned} \tag{71}$$

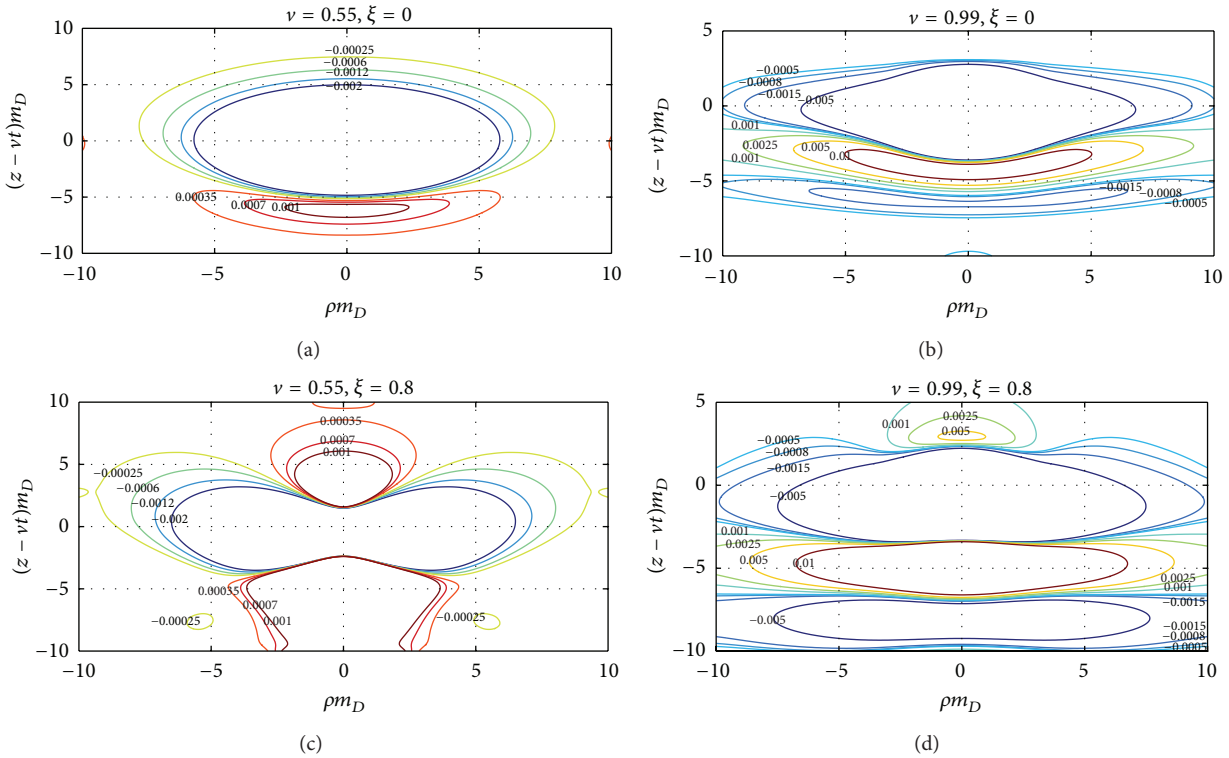

FIGURE 10: (Color online) Left Panel: the plot shows equicharge line with parton velocity $v = 0.55$ for different $\xi(0, 0.8)$. Right Panel: same as left panel with parton velocity $v = 0.99$.

with $\Omega = k(z\chi + (\rho - vt)\sqrt{1-\chi^2}\cos\phi)m_D$. Numerical results of the equicharge lines are shown in Figure 11. The left (right) panel shows the contour plots of the induced charge density for the parton velocity $v = 0.55(0.99)$. When $v = 0.99$, the number of induced charge lines that appear alternately in the backward space is reduced for the anisotropic plasma in comparison to the isotropic plasma. Therefore, the anisotropy reduces the oscillatory behavior of the induced color charge density when the parton moves perpendicular to the anisotropy direction.

According to the Poisson equation, the wake potential induced by the fast parton reads as [33]

$$\Phi^a(\mathbf{k},\omega) = \frac{\rho^a_{\text{ext}}(\mathbf{k},\omega)}{k^2\epsilon(\mathbf{k},\omega)}. \tag{72}$$

Substituting (68) into (72) and transforming to the configuration space, the wake potential is given by [38]

$$\Phi^a(\mathbf{r},t) = 2\pi Q^a \int \frac{d^3k}{(2\pi)^3}\int\frac{d\omega}{2\pi}\exp^{i(\mathbf{k}\cdot\mathbf{r}-\omega t)}\frac{1}{k^2\epsilon(\omega,\mathbf{k})}\delta(\omega-\mathbf{k}\cdot\mathbf{v}). \tag{73}$$

Using similar coordinate system as before, the screening potential turns into

$$\Phi^a(\mathbf{r},t) = \frac{Q^a m_D}{2\pi^2}\int_0^\infty dk \times \int_0^1 d\chi\, J_0\left(k\rho\sqrt{1-\chi^2}m_D\right) \times\left[\cos\Gamma\frac{\text{Re}\,\epsilon(\omega,\mathbf{k})}{\Delta} + \sin\Gamma\frac{\text{Im}\,\epsilon(\omega,\mathbf{k})}{\Delta}\right]\Bigg|_{\omega=\mathbf{k}\cdot\mathbf{v}}. \tag{74}$$

We solve the wake potential for the two special cases: (i) along the parallel direction of the fast parton, that is, $\mathbf{r} \parallel \mathbf{v}$ and also $\rho = 0$ and (ii) perpendicular to direction of the parton, that is, $\mathbf{r} \perp \mathbf{v}$. The potential for the parallel case is obtained as

$$\Phi^a_{\parallel}(\mathbf{r},t) = \frac{Q^a m_D}{2\pi^2}\int_0^\infty dk \times\int_0^1 d\chi\left[\cos\Gamma\frac{\text{Re}\,\epsilon(\omega,\mathbf{k})}{\Delta} + \sin\Gamma\frac{\text{Im}\,\epsilon(\omega,\mathbf{k})}{\Delta}\right]\Bigg|_{\omega=\mathbf{k}\cdot\mathbf{v}}, \tag{75}$$

whereas that for the perpendicular case, we have

$$\Phi^a_{\perp}(\mathbf{r},t) = \frac{Q^a m_D}{2\pi^2}\int_0^\infty dk \times\int_0^1 d\chi\, J_0\left(k\rho\sqrt{1-\chi^2}m_D\right)$$

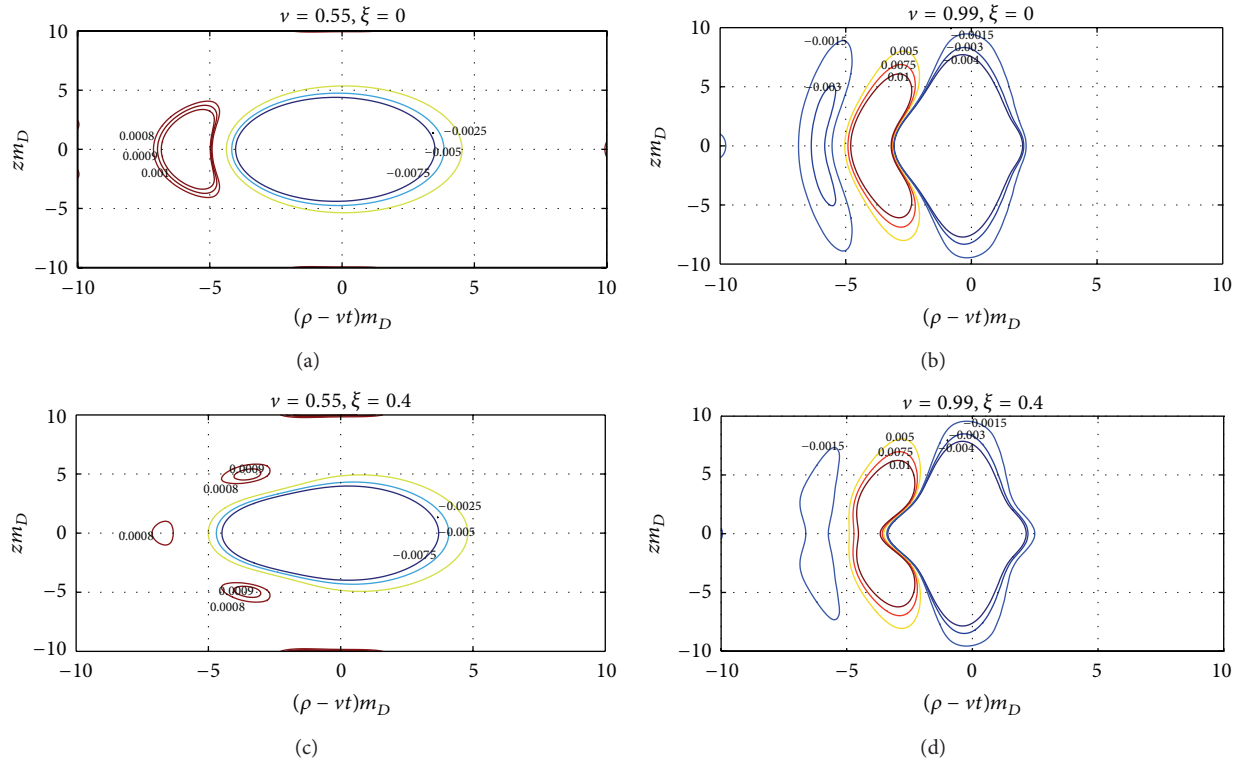

FIGURE 11: (Color online) The left (right) panel shows the equicharge lines for $v = 0.55(0.99)$. In this case the parton moves perpendicular to the direction of anisotropy [38].

$$\times \left[\cos\Gamma' \frac{\mathrm{Re}\,\epsilon(\omega,\mathbf{k})}{\Delta} - \sin\Gamma' \frac{\mathrm{Im}\,\epsilon(\omega,\mathbf{k})}{\Delta} \right]\Bigg|_{\omega=\mathbf{k}\cdot\mathbf{v}}, \tag{76}$$

with $\Gamma' = k\chi v t m_D$.

Figure 12 describes the scaled wake potential in two specified directions. In these figures, the scaled parameter Φ_0^a is given by $(2\pi^2/m_D)\Phi^a$. The left panel shows the wake potential along the direction of the moving color charge. In the backward direction, the wake potential for isotropic plasma decreases with the increase of $z - vt$ and exhibits a negative minimum when $v = 0.55$. With the increase of the anisotropic parameter ξ, the depth of the negative minimum decreases for $v = 0.55$. At large $\xi(0.8)$, there is no negative minimum and the wake potential behaves like a modified Coulomb potential. For $v = 0.99$, the wake potential is Lennard-Jones potential type which has a short range repulsive part as well as a long range attractive part [34, 38] in both isotropic and anisotropic plasma. It is also seen that the wake potential is oscillatory in nature in the backward direction. It is clearly visible that the depth of the negative minimum is increased compared to the case when $v = 0.55$. Because of the anisotropy effect, the oscillation of the wake potential is more pronounced, and it extends to a large distance [38]. In the forward direction, the screening potential is a modified Coulomb potential in both types of plasma. Figure 12(b) describes the wake potential along the perpendicular direction of the moving parton. It can be seen that the wake potential is symmetric in backward and forward direction, no matter what the speed is [38]. In presence of the moving charge particle, the wake potential is Lennard-Jones type. When $v = 0.55$, the value of negative minimum is increased with increase of ξ but in case of $v = 0.99$, it decreases with ξ. However, with the increase of ξ, the depth of negative minimum is moving away from the origin for both the jet velocities considered here.

Next, we consider the case when the parton moves perpendicular to the beam direction. The wake potential in (74) is also evaluated for the two spacial cases: (i) along the direction of the moving parton, that is, $\mathbf{r} \parallel \mathbf{v}$ and (ii) perpendicular direction of the parton, that is, $\mathbf{r} \perp \mathbf{v}$. The wake potential for the parallel case can be written as [38]

$$\Phi_{\parallel}^a(\mathbf{r},t) = \frac{Q^a m_D}{2\pi^2} \int_0^\infty dk \int_0^1 d\chi \times \int_0^{2\pi} \frac{d\phi}{2\pi} \times \left[\cos\Omega' \frac{\mathrm{Re}\,\epsilon(\omega,\mathbf{k})}{\Delta} + \sin\Omega' \frac{\mathrm{Im}\,\epsilon(\omega,\mathbf{k})}{\Delta} \right]\Bigg|_{\omega=\mathbf{k}\cdot\mathbf{v}}, \tag{77}$$

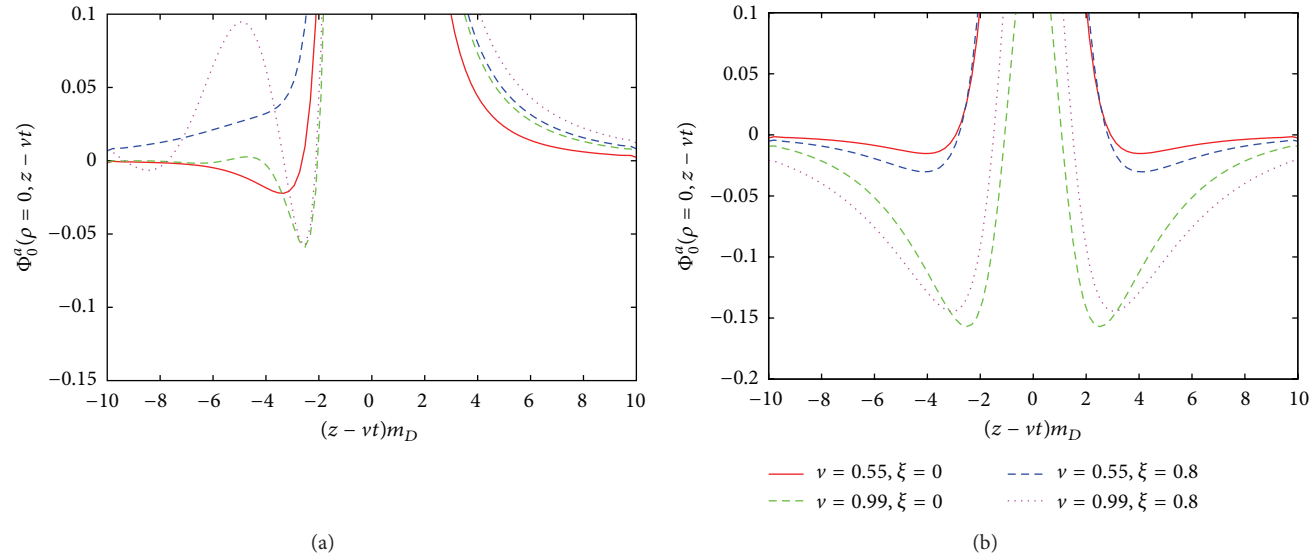

FIGURE 12: (Color online) (a): scaled wake potential along the motion of the fast parton, that is, z-axis for different ξ with two different parton velocity $v = 0.55$ and $v = 0.99$. (b) same as (a) but perpendicular to direction of motion of the parton.

where $\Omega' = k(\rho - vt)\sqrt{1-\chi^2}\cos\phi m_D$. For the perpendicular case it is given by

$$\Phi_\perp^a(\mathbf{r}, t) = \frac{Q^a m_D}{2\pi^2}\int_0^\infty dk \int_0^1 d\chi \times \int_0^{2\pi}\frac{d\phi}{2\pi} \times \left[\cos\Omega''\frac{\mathrm{Re}\,\epsilon(\omega, \mathbf{k})}{\Delta} + \sin\Omega''\frac{\mathrm{Im}\,\epsilon(\omega, \mathbf{k})}{\Delta}\right]\Bigg|_{\omega=\mathbf{k}\cdot\mathbf{v}}, \tag{78}$$

with $\Omega'' = k(z\chi - vt\sqrt{1-\chi^2}\cos\phi)m_D$. The left panel in Figure 13 shows screening potential along the parallel direction of the moving color charge. The behavior of the wake potential is more like a modified Coulomb (Lennard-Jones) potential at parton velocity $v = 0.55(0.99)$. For $v = 0.99$, the wake potential shows an oscillatory behavior in an isotropic plasma [34] but in anisotropic case, oscillatory structure of the wake potential is smeared out for $\xi = 0.5$ and $\mathbf{v} \perp \hat{\mathbf{n}}$ [38]. But the depth of the negative minimum increases in the case of anisotropic plasma for both the parton velocities considered here. The behavior of the wake potential in the perpendicular direction of the moving parton is shown in the right panel of Figure 13. At $v = 0.55$, the anisotropy modifies the structure of the wake potential significantly, that is, it becomes modified Coulomb potential instead of Lennard-Jones potential. For $v = 0.99$, the wake potential is a Lennard-Jones potential type but the depth of the minimum decreases in anisotropic plasma [38].

6. Summary and Discussions

We have reviewed the effect of initial state momentum anisotropy that can arise in an AQGP on various observables. It is shown that electromagnetic probes could be a good signal that can be used to characterize this anisotropic state as this can only be realized in the early stages of heavy ion collisions. It has been demonstrated that the isotropization time of the QGP can be extracted by comparing the photon yield with the experimental data. We further estimate the radiative energy loss of a fast moving parton (both heavy and light flavours) in an AQGP and show that the it is substantially different from that in the isotropic QGP. Moreover, it depends on the direction of propagation of the parton with the anisotropic axis. Related to this is the nuclear modification factor of light hadrons that is produced due to the fragmentation of light partons which lose energy in the medium. Thus,we have also discussed the nuclear modification factor in the context of AQGP and compared it with the RHIC data to extract the isotropization time. The extracted value is compatible with that obtained from photon data.

It might be mentioned here that the presence of unstable modes in AQGP may affect radiative energy loss. However, in [72, 73] the authors have shown that the polarization loss (collisional loss) remains unaffected by the unstable modes, but in a recent paper [74] it is shown that the polarisation loss indeed has strong time and directional dependence and also the nature of the loss is oscillatory. Such effect may be present in radiative energy loss. In this review, we did not consider it.

The heavy quark potential and the quarkonium states in AQGP have also been reviewed with both real and complex valued potential. In all these calculations, it has been found that the dissociation temperature of various quarkonium states increases in comparison with the isotropic case. We have also focused on the nuclear modification factors of various bottomonium states which have been calculated by

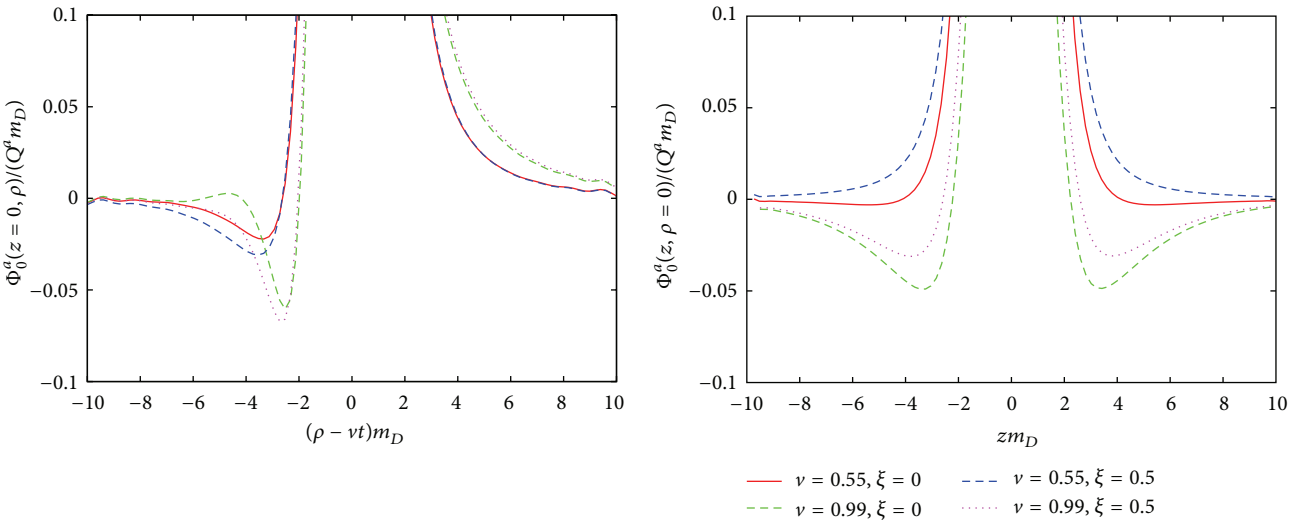

(a) (b)

FIGURE 13: (Color online) The left (right) panel shows scaled wake potential for $\xi = \{0, 0.5\}$ with parton velocity $v = 0.55(0.99)$. In this case the parton moves perpendicular to the direction of anisotropy [38].

combining hydrodynamics and solutions of 3D Schrodinger equation using two types of complex valued potentials.

Apart from the energy loss of a jet in a medium, the jet also creates wake in the plasma. We have demonstrated that due to the jet propagation in an AQGP, the wake potential and the charge density are significantly modified in comparison with the isotropic case.

We end by mentioning that the ADS/CFT calculation of the electromagnetic correlator has been performed in strongly coupled $\mathcal{N} = 4$ super Yang-Mills theory using anisotropic momentum distribution [75]. Photon production rate is then estimated and it is concluded that in the weak coupling limit, the rate is consistent with that in [41] with an oblate phase space distribution in momentum space. There are other models that deal with the gravity dual theory for anisotropic plasma with additional bulk fields [76, 77]. Thus, a comparative study of various observables in gravity dual theory should be done in the future.

References

[1] J.-E. Alam, S. Sarkar, P. Roy, T. Hatsuda, and B. Sinha, "Thermal photons and lepton pairs from quark gluon plasma and hot hadronic matter," *Annals of Physics*, vol. 286, no. 2, pp. 159–248, 2000.

[2] H. Satz and T. Matsui, "J/ψ suppression by quark-gluon plasma formation," *Physics Letters B*, vol. 178, no. 4, pp. 416–422, 1986.

[3] J. D. Bjorken, "Partons lose energy due to interactions with the medium," *FERMILAB-Pub-82/59-THY*, Erratum, 1982.

[4] M. Gyulassy, P. Levai, and I. Vitev, "Jet quenching in thin quark-gluon plasmas I: formalism," *Nuclear Physics B*, vol. 571, pp. 197–233, 2000.

[5] B. G. Zakharov, "On the energy loss of high energy quarks in a finite-size quark-gluon plasma," *JETP Letters*, vol. 73, no. 2, pp. 49–52, 2001.

[6] M. Djordjevic and U. Heinz, "Radiative energy loss in a finite dynamical QCD medium," *Physical Review Letters*, vol. 101, no. 2, Article ID 022302, 4 pages, 2008.

[7] G.-Y. Qin, J. Ruppert, C. Gale, S. Jeon, G. D. Moore, and M. G. Mustafa, "Radiative and collisional jet energy loss in the quark-gluon plasma at the BNL relativistic heavy ion collider," *Physical Review Letters*, vol. 100, no. 7, Article ID 072301, 2008.

[8] R. Baier, Y. L. Dokshitzer, A. H. Mueller, and D. Schiff, "Quenching of hadron spectra in media," *Journal of High Energy Physics*, vol. 2001, article 033, 2001.

[9] A. K. Dutt-Mazumder, J. Alam, P. Roy, and B. Sinha, "Stopping power of hot QCD plasma," *Physical Review D*, vol. 71, no. 9, Article ID 094016, 9 pages, 2005.

[10] P. Roy, J.-E. Alam, and A. K. Dutt-Mazumder, "Quenching of light hadrons at RHIC in a collisional energy loss scenario," *Journal of Physics G*, vol. 35, no. 10, Article ID 104047, 2008.

[11] P. Huovinen, P. Kolb, U. Heinz, and P. V. Ruuskanen, "Radial and elliptic flow at RHIC: further predictions," *Physics Letters B*, vol. 503, no. 1-2, pp. 58–64, 2001.

[12] T. Hirano and K. Tsuda, "Collective flow and two-pion correlations from a relativistic hydrodynamic model with early chemical freeze-out," *Physical Review C*, vol. 66, no. 5, Article ID 054905, 14 pages, 2002.

[13] M. J. Tannenbaum, "Recent results in relativistic heavy ion collisions: from 'a new state of matter' to 'the perfect fluid'," *Reports on Progress in Physics*, vol. 69, no. 7, 2005.

[14] M. Luzum and P. Romatschke, "Conformal relativistic viscous hydrodynamics: applications to RHIC results at $\sqrt{s_{NN}} = 200$ GeV," *Physical Review C*, vol. 78, no. 3, Article ID 034915, 17 pages, 2008.

[15] M. Mandal and P. Roy, "Gluon dissociation of J/ψ in anisotropic quark-gluon plasma," *Physical Review C*, vol. 86, no. 2, Article ID 024915, 7 pages, 2012.

[16] L. Bhattacharya and P. Roy, "Measuring the isotropization time of quark-gluon plasma from direct photons at energies available at the BNL Relativistic Heavy Ion Collider (RHIC)," *Physical Review C*, vol. 79, no. 5, Article ID 054910, 7 pages, 2009.

[17] M. Martinez and M. Strickland, "Dilepton production as a measure of QGP thermalization time," *Journal of Physics G*, vol. 35, no. 10, Article ID 104162, 2008.

[18] R. Baier, A. H. Muller, D. Schiff, and D. T. Son, "'Bottom-up' thermalization in heavy ion collisions," *Physics Letters B*, vol. 502, no. 1–4, pp. 51–58, 2001.

[19] E. Webel, "Spontaneously growing transverse waves in a plasma due to an anisotropic velocity distribution," *Physical Review Letters*, vol. 2, no. 3, p. 83, 1959.

[20] S. Mrowczynski, "Plasma instability at the initial stage of ultrarelativistic heavy-ion collisions," *Physics Letters B*, vol. 314, no. 1, pp. 118–121, 1993.

[21] S. Mrowczynski, "Color collective effects at the early stage of ultrarelativistic heavy-ion collisions," *Physical Review C*, vol. 49, no. 4, pp. 2191–2197, 1994.

[22] S. Mrowczynski, "Color filamentation in ultrarelativistic heavy-ion collisions," *Physics Letters B*, vol. 393, no. 1-2, pp. 26–30, 1997.

[23] S. Mrowczynski, "Instabilities driven equilibration of the quark—gluon plasma," *Acta Physica Polonica B*, vol. 37, pp. 427–454, 2006.

[24] P. Arnold, J. Lenghan, G. D. Moore, and L. G. Yaffe, "apparent thermalization due to plasma instabilities in the quark-gluon plasma," *Physical Review Letters*, vol. 94, no. 7, Article ID 072302, 4 pages, 2005.

[25] A. Rebhan, P. Romatschke, and M. Strickland, "Hard-loop dynamics of non-abelian plasma instabilities," *Physical Review Letters*, vol. 94, no. 10, Article ID 102303, 4 pages, 2005.

[26] P. Romatschke and R. venugopalan, "Collective non-abelian instabilities in a melting color glass condensate," *Physical Review Letters*, vol. 96, no. 6, Article ID 062302, 4 pages, 2006.

[27] M. Strickland, "The chromo-weibel instability," *Brazilian Journal of Physics*, vol. 37, no. 2, p. 702, 2007.

[28] P. Romatschke and M. Strickland, "Collective modes of an anisotropic quark-gluon plasma," *Physical Review D*, vol. 68, no. 3, Article ID 036004, 8 pages, 2003.

[29] P. Romatschke and M. Strickland, "Collective modes of an anisotropic quark-gluon plasma: II," *Physical Review D*, vol. 70, no. 11, Article ID 116006, 9 pages, 2004.

[30] P. Romatschke and M. Stricland, "Collisional energy loss of a heavy quark in an anisotropic quark-gluon plasma," *Physical Review D*, vol. 71, no. 12, Article ID 125008, 2005.

[31] P. Romatschke, "Momentum broadening in an anisotropic plasma," *Physical Review C*, vol. 75, no. 1, Article ID 014901, 8 pages, 2007.

[32] P. Roy and A. K. Dutt-Mazumder, "Radiative energy loss in an anisotropic quark-gluon plasma," *Physical Review C*, vol. 83, no. 4, Article ID 044904, 6 pages, 2011.

[33] J. Ruppert and B. Muller, "Waking the colored plasma," *Physics Letters B*, vol. 618, no. 1–4, pp. 123–130, 2005.

[34] P. Chakraborty, M. G. Mustafa, and M. H. Thoma, "Wakes in the quark-gluon plasma," *Physical Review D*, vol. 74, no. 9, Article ID 094002, 16 pages, 2006.

[35] P. Chakraborty, M. G. Mustafa, R. Ray, and M. H. Thoma, "Wakes in a collisional quark-gluon plasma," *Journal of Physics G*, vol. 34, no. 10, p. 2141, 2007.

[36] B.-F. Jiang and J.-R. Li, "The wake potential in the viscous quark-gluon plasma," *Nuclear Physics A*, vol. 856, no. 1, pp. 121–133, 2011.

[37] B.-f. Jiang and J.-r. Li, "The polarized charge distribution induced by a fast parton in the viscous quark-gluon plasma," *Journal of Physics G*, vol. 39, no. 2, Article ID 025007, 2012.

[38] M. Mandal and P. Roy, "Wake in anisotropic quark-gluon plasma," *Physical Review D*, vol. 86, no. 11, Article ID 114002, 9 pages, 2012.

[39] L. Bhattacharya and P. Roy, "Photons from anisotropic quark-gluon plasma," *Physical Review C*, vol. 78, no. 6, Article ID 064904, 2008.

[40] L. Bhattacharya and P. Roy, "Rapidity distribution of photons from an anisotropic quark-gluon plasma," *Physical Review C*, vol. 81, no. 5, Article ID 054904, 2010.

[41] B. Schenke and M. Stricland, "Photon production from an anisotropic quark-gluon plasma," *Physical Review D*, vol. 76, no. 2, Article ID 025023, 5 pages, 2007.

[42] M. Martinez and M. Strickland, "Measuring quark-gluon-plasma thermalization time with dileptons," *Physical Review Letters*, vol. 100, no. 10, Article ID 102301, 4 pages, 2008.

[43] M. Martinez and M. Strickland, "Pre-equilibrium dilepton production from an anisotropic quark-gluon plasma," *Physical Review C*, vol. 78, no. 3, Article ID 034917, 19 pages, 2008.

[44] M. Mandal, L. Bhattacharya, and P. Roy, "Nuclear modification factor in an anisotropic quark-gluon plasma," *Physical Review C*, vol. 84, no. 4, Article ID 044910, 10 pages, 2011.

[45] M. Martinez and M. Strickland, "Dissipative dynamics of highly anisotropic systems," *Nuclear Physics A*, vol. 848, no. 1-2, pp. 183–197, 2010.

[46] M. Martinez and M. Strickland, "Non-boost-invariant anisotropic dynamics," *Nuclear Physics A*, vol. 856, no. 1, pp. 68–87, 2011.

[47] K. Kajantie, J. Kapusta, L. McLerran, and A. Mekjian, "Dilepton emission and the QCD phase transition in ultrarelativistic nuclear collisions," *Physical Review D*, vol. 34, no. 9, pp. 2746–2754, 1986.

[48] A. Dumitru, Y. Guo, and M. Strickland, "The heavy-quark potential in an anisotropic plasma," *Physics Letters B*, vol. 662, no. 1, pp. 37–42, 2008.

[49] J. P. Blaizot and E. Iancu, "The quark-gluon plasma: collective dynamics and hard thermal loops," *Physics Reports*, vol. 359, no. 5-6, pp. 155–528, 2002.

[50] B. Schenke, M. Strickland, C. Greiner, and M. Thoma, "Model of the effect of collisions on QCD plasma instabilities," *Physical Review D*, vol. 73, no. 12, Article ID 125004, 12 pages, 2006.

[51] A. Dumitru, Y. Gao, A. Mocsy, and M. Strickland, "Quarkonium states in an anisotropic QCD plasma," *Physical Review D*, vol. 79, no. 5, Article ID 054019, 10 pages, 2009.

[52] F. Karsch, M. T. Mehr, and H. Satz, "Color screening and deconfinement for bound states of heavy quarks," *Zeitschrift für Physik C*, vol. 37, no. 4, pp. 617–622, 1988.

[53] I. D. Sudiarta and D. J. W. Geldart, "Solving the Schrödinger equation using the finite difference time domain method," *Journal of Physics A*, vol. 40, no. 8, pp. 1885–1896, 2007.

[54] M. Margotta, K. McCarty, C. McGahan, M. Strickland, and D. Yager-Elorriaga, "Quarkonium states in a complex-valued potential," *Physical Review D*, vol. 83, Article ID 105019, 2011.

[55] A. Dumitru, Y. Gao, and M. Strickland, "Imaginary part of the static gluon propagator in an anisotropic (viscous) QCD plasma," *Physical Review D*, vol. 79, no. 11, Article ID 114003, 7 pages, 2009.

[56] M. Strickland, "Thermal $\Upsilon(1_s)$ and χ_{b1} Suppression at $\sqrt{(s_{NN})} = 2.76$ TeV Pb-Pb Collisions at the LHC," *Physical Review Letters*, vol. 107, no. 13, Article ID 132301, 4 pages, 2011.

[57] M. Strickland and D. Bazow, "Thermal bottomonium suppression at RHIC and LHC," *Nuclear Physics A*, vol. 879, pp. 25–58, 2012.

[58] X.-M. Xu, D. Kharzeev, H. Satz, and X.-N. Wang, "J/ψ suppression in an equilibrating parton plasma," *Physical Review C*, vol. 53, no. 6, pp. 3051–3056, 1996.

[59] G. Bhanot and M. E. Peskin, "Short-distance analysis for heavy-quark systems. (II). Applications," *Nuclear Physics B*, vol. 156, no. 3, pp. 391–416, 1979.

[60] D. Kharzeev and H. Satz, "Colour deconfinement and quarkonium dissociation," in *Quark-Gluon Plasma II*, R. C. Hwa, Ed., World Scientific, Singapore, 1995.

[61] M. Gyulassy and X. N. Wang, "Multiple collisions and induced gluon bremsstrahlung in QCD," *Nuclear Physics B*, vol. 420, no. 3, pp. 583–614, 1994.

[62] M. Djordjevic, "Theoretical formalism of radiative jet energy loss in a finite size dynamical QCD medium," *Physical Review C*, vol. 80, no. 6, Article ID 064909, 27 pages, 2009.

[63] J. F. Owens, "Large-momentum-transfer production of direct photons, jets, and particles," *Reviews of Modern Physics*, vol. 59, no. 2, pp. 465–503, 1987.

[64] P. Roy, A. K. Dutt-Mazumder, and J.-E. Alam, "Energy loss and dynamical evolution of quark p_T spectra," *Physical Review C*, vol. 73, no. 4, Article ID 044911, 4 pages, 2006.

[65] X. N. Wang, "Effects of jet quenching on high p_T hadron spectra in high-energy nuclear collisions," *Physical Review C*, vol. 58, no. 4, pp. 2321–2330, 1998.

[66] S. Turbide, C. Gale, S. Jeon, and G. D. Moore, "Energy loss of leading hadrons and direct photon production in evolving quark-gluon plasma," *Physical Review C*, vol. 72, no. 1, Article ID 014906, 15 pages, 2005.

[67] S. S. Adler, S. Afanasiev, C. Aidala et al., "Common suppression pattern of η and π^0 mesons at high transverse momentum in Au+Au collisions at $\sqrt{(s_{NN})} = 200$ GeV," *Physical Review Letters*, vol. 96, no. 20, Article ID 202301, 6 pages, 2006.

[68] N. A. Krall and A. W. Trivilpiece, *Principles of Plasma Physics*, McGraw-Hill, New York, NY, USA, 1973.

[69] S. Ichimaru, *Basic Principles of Plasma Physics*, W. A. Benjamin, Menlo Park, Calif, USA, 1973.

[70] L. D. Landau and E. M. Lifshitz, *Fluid Mechanics*, Butterworth-Heinemann, Woburn, Mass, USA, 2nd edition, 1987.

[71] W. J. Miloch, "Wake effects and Mach cones behind objects," *Plasma Physics and Controlled Fusion*, vol. 52, no. 12, Article ID 124004, 2010.

[72] P. Romatschke and M. strickland, "Energy loss of a heavy fermion in an anisotropic QED plasma," *Physical Review D*, vol. 69, no. 6, Article ID 065005, 13 pages, 2005.

[73] P. Romatschke and M. strickland, "Collisional energy loss of a heavy quark in an anisotropic quark-gluon plasma," *Physical Review D*, vol. 71, no. 12, Article ID 125008, 12 pages, 2005.

[74] M. E. Carrington, K. Deja, and S. Mrówczyński, "Energy loss in unstable quark-gluon plasma with extremely prolate momentum distribution," *Acta Physica Polonica B*, vol. 6, supplement, p. 545, 2013.

[75] A. Rebhan and D. Steineder, "Electromagnetic signatures of a strongly coupled anisotropic plasma," *Journal of High Energy Physics*, vol. 2011, article 153, 2011.

[76] D. Mateos and D. Trancanelli, "Anisotropic $N = 4$ Super-Yang-Mills Plasma and Its Instabilities," *Physical Review Letters*, vol. 107, no. 10, 4 pages, 2011.

[77] D. Mateos and D. Trancanelli, "Thermodynamics and instabilities of a strongly coupled anisotropic plasma," *Journal of High Energy Physics*, vol. 2011, article 54, 2011.